Available online at www.sciencedirect.com
SCIENCE DIRECT®
Geochimica et Cosmochimica Acta 70 (2006) 2006–2022
Geochimica
www.elsevier.com/locate/gca

The effect of early diagenesis on the Fe isotope compositions of porewaters and authigenic minerals in continental margin sediments

Silke Severmann [a,*], Clark M. Johnson [a], Brian L. Beard [a], James McManus [b]

[a] Department of Geology and Geophysics, University of Wisconsin, Madison, WI 53706, USA
[b] College of Oceanic and Atmospheric Sciences, Oregon State University, Corvallis, OR 97331, USA

Received 15 October 2004; accepted in revised form 11 January 2006

Abstract

Iron isotope compositions in marine pore fluids and sedimentary solid phases were measured at two sites along the California continental margin, where isotope compositions range from $\delta^{56}Fe = -3.0‰$ to $+0.4‰$. At one site near Monterey Canyon off central California, organic matter oxidation likely proceeds through a number of diagenetic pathways that include significant dissimilatory iron reduction (DIR) and bacterial sulfate reduction, whereas at our other site in the Santa Barbara basin DIR appears to be comparatively small, and production of sulfides (FeS and pyrite) was extensive. The largest range in Fe isotope compositions is observed for $Fe(II)_{aq}$ in porewaters, which generally have the lowest $\delta^{56}Fe$ values (minimum: $-3.0‰$) near the sediment surface, and increase with burial depth. $\delta^{56}Fe$ values for FeS inferred from HCl extractions vary between $\sim -0.4‰$ and $+0.4‰$, but pyrite is similar at both stations, where an average $\delta^{56}Fe$ value of $-0.8 \pm 0.2‰$ was measured. We interpret variations in dissolved Fe isotope compositions to be best explained by open-system behavior that involves extensive recycling of Fe. This study is the first to examine Fe isotope variations in modern marine sediments, and the results show that Fe isotopes in the various reactive Fe pools undergo isotopic fractionation during early diagenesis. Importantly, processes dominated by sulfide formation produce high-$\delta^{56}Fe$ values for porewaters, whereas the opposite occurs when Fe(III)-oxides are present and DIR is a major pathway of organic carbon respiration. Because shelf pore fluids may carry a negative $\delta^{56}Fe$ signature it is possible that the Fe isotope composition of ocean water reflects a significant contribution of shelf-derived iron to the open ocean. Such a signature would be an important means for tracing iron sources to the ocean and water mass circulation.

1. Introduction

The geochemical behavior of transition metals, particularly those that occur in multiple oxidation states, has long attracted attention as tracers of abiotic and biologically controlled redox-transformations in marine sediments (e.g., Froelich et al., 1979; Sørensen and Jørgensen, 1987; Shaw et al., 1990; Lapp and Balzer, 1993; Thamdrup et al., 1994; Thomson et al., 1996; Morford and Emerson, 1999). The chemistry of Fe in organic-rich sediments is of particular interest because Fe chemistry controls the distribution of dissolved sulfide, the solubility of many trace metals, and burial rates of phosphorus in sediments (Pyzik and Sommer, 1981; Ruttenberg and Berner, 1993; Morse, 1994). In addition, the chemistry of Fe in the oceans plays an important role in controlling primary production in the surface ocean (Martin, 1990), and the delivery of dissolved Fe from coastal or shallow margin marine sediments to the water column could account for as much as 50% of the global Fe input to the oceans (e.g., Elrod et al., 2004). On a regional scale, the benthic Fe flux could account for all of the required Fe necessary to support new production (Berelson et al., 2003). Thus, given the importance of this micronutrient and the importance of coastal sediments for Fe input, it would be appealing to develop a tracer for coastal sedimentary Fe flux. Some of the major challenges with respect to the role of Fe cycling in coastal

* Corresponding author. Present address: Department of Earth Sciences, University of California Riverside, Riverside, CA 92521, USA. Fax: +1 951 827 4324.
E-mail address: Silke.Severmann@ucr.edu (S. Severmann).

0016-7037/$ - see front matter © 2006 Elsevier Inc. All rights reserved.
doi:10.1016/j.gca.2006.01.007

environments concern quantifying rates of dissimilatory iron reduction (DIR) in marine sediments (Canfield and Des Marais, 1993; Thamdrup, 2000), and the relative contributions of Fe fluxes from continental margin environments to the open ocean (Laës et al., 2003; Elrod et al., 2004).

The field of Fe isotope geochemistry is growing rapidly, and isotopic fractionations of up to ~5‰ in $^{56}Fe/^{54}Fe$ ratios have been measured in natural samples (Zhu et al., 2000; Bullen et al., 2001; Sharma et al., 2001; Beard et al., 2003b; Beard and Johnson, 2004; Johnson et al., 2003; Rouxel et al., 2003, 2004, 2005; Levasseur et al., 2004; Matthews et al., 2004; Severmann et al., 2004; Yamaguchi et al., 2005). In contrast to the range in Fe isotope compositions of rocks and fluids that involve Fe cycling or precipitation of minerals at moderate to low temperature, the isotopic compositions of igneous rocks and low organic carbon clastic rocks are relatively homogeneous (C_{org}) (Beard et al., 2003a,b; Yamaguchi et al., 2005).

Because of the variability in isotopic compositions and the potential usefulness of Fe isotopes as a proxy for Fe biogeochemical processing, a number of studies have targeted biological processing during oxidation and reduction (Beard et al., 1999; Beard et al., 2003a; Croal et al., 2004; Icopini et al., 2004; Johnson et al., 2004; Crosby et al., 2005; Johnson et al., 2005). In addition to metabolic processing of Fe, isotopic fractionation may also occur through abiotic processes that are relevant to natural systems (Brantley et al., 2001; Bullen et al., 2001; Johnson et al., 2002; Skulan et al., 2002; Welch et al., 2003; Brantley et al., 2004; Wiesli et al., 2004). The largest fractionations in abiotic and biotic systems occur between oxidized and reduced phases of Fe, where ferric Fe species tend to have the highest $^{56}Fe/^{54}Fe$ ratios (Polyakov and Mineev, 2000; Schauble et al., 2001; Johnson et al., 2002; Welch et al., 2003; Anbar et al., 2005).

In this study, we examine the isotopic systematics of aqueous and solid Fe phases in modern sediments from the California continental margin. In particular, analysis of porewaters allows us to *directly* assess the Fe isotope composition of the benthic Fe flux in a classic continental shelf setting. Partial extractions of different solid components are used to assess mineral transformation reactions and to evaluate fluid–mineral isotope fractionations in a natural, biologically active sedimentary environment. These results provide important constraints on the mechanisms and pathways involved in producing Fe isotope variations in diagenetic environments. Understanding how these Fe isotope variations are expressed in modern sediments is necessary for interpretation of Fe isotope variations in the ancient rock record and their potential for re-construction of ocean–atmosphere interactions throughout the Archean and Proterozoic (Rouxel et al., 2005).

2. Study sites

The two study sites reside along the highly productive eastern boundary of the North Pacific from central to southern California (Table 1). The first site in the Monterey Canyon (MC) is located near Monterey Bay at a water depth of ~450 m. Sediments in this region are generally sandy muds, dark green in color, and often support abundant macrofauna that promote intense bioturbation and bioirrigation (Berelson et al., 2003). Primary productivity in the region typically ranges from 40 to 220 mmol C m^{-2} day^{-1} (during non-El Niño years), and carbon rain rates at 450 m depth range from 0.8 to 10 mmol C m^{-2} day^{-1} (Table 1; Pilskaln et al., 1996). Sediment trap data from 450 meters depth (Pilskaln et al., 1996) and incubation chamber deployments from multiple locations in this general area (Berelson et al., 2003) point to seasonal variability in the sea floor organic carbon oxidation rate, ranging from 6 to 12 mmol C m^{-2} day^{-1}. Although we did not measure organic carbon concentrations at our sites, organic carbon contents range from 0.2 to 0.5 dry weight percent (dwt.%) from a nearby site in Monterey Bay (Berelson et al., 2003).

The second sampling site is located near the sill within the Santa Barbara basin (SBB), which has the lowest bottom water oxygen concentrations of the submarine California borderland basins, although the bottom water rarely turns fully anoxic (Reimers et al., 1996). The cores studied here were recovered from the slope of the basin at 498 m water depth, where bottom water oxygen is typically ~10 μM O_2 (Zheng et al., 2000). The sediments are com-

Table 1
Sample locations, water depth and bottom water oxygen concentrations of California Margin sites discussed in this study

Location Name	Latitude/longitude	Water depth (m)	Bottom water oxygen (μM)	Carbon rain rate (mmol m^{-2} day^{-1})	Organic carbon concentration (% dwt.)
Monterey Canyon	36° 47.67′ N 121° 53.65′ W	450	>100[a]	0.8–10[c]	0.2–0.5[a]
Santa Barbara basin	34° 16.87′ N 119° 54.84′ W	496	~10[b]	~6[d]	2.1–2.6[e]

[a] Data for Monterey Bay from Berelson et al. (2003).
[b] Data from Zheng et al. (2000).
[c] Data for Monterey Bay from Pilskaln et al. (1996).
[d] Data from Zheng et al. (2000) and Thunell et al. (1995).
[e] Data from Sholkovitz (1973).

prised of fine-grained clays and silts that are dark brown to black in color, and typical organic carbon contents range from 2.1 to 2.6 dwt.% (Sholkovitz, 1973), higher than those expected at MC. The organic carbon rain rate, however, is comparable between the two sites, where fluxes of $\sim$6 mmol C m^{-2} day^{-1} were measured by Zheng et al. (2000) and Thunell et al. (1995) at the SBB locality (Table 1).

3. Methods

3.1. Sample collection and elemental analysis

Sediments and porewaters were collected in June and July 2003 on board the R/V Point Sur. Undisturbed surface sediments were sampled using a multi-corer, and concomitant deeper sediments were sampled using a gravity corer. Upon recovery, sediment cores were placed immediately into N_2-filled glove bags, where they were processed within 1 h at approximately bottom water temperature ($\sim$5 °C). Porewaters were isolated by centrifugation and filtered under nitrogen through 0.45 μm cellulose-acetate filters. Small sub-samples of filtered porewater were reacted with 10% Zn-acetate solution to fix H_2S as ZnS (total dissolved sulfide is collectively termed ΣH_2S). A second aliquot was used for ammonia analysis. The remaining porewaters were acidified with ultra-pure 6 M HCl to pH <2 for analysis of dissolved metal concentrations and Fe isotope compositions. A portion of the centrifuged sediments was stored frozen for solid phase analysis.

Ammonia and ΣH_2S analysis were performed at sea generally within 24 h of sample collection, using standard spectrophotometrical techniques (Cline, 1969; Parsons et al., 1984). Only gravity cores were analyzed for ΣH_2S. The analytical uncertainties for ΣH_2S and ammonia were 1 and 0.2 μM, respectively (1-SD). Dissolved total Fe and Mn were analysed by graphite-furnace atomic absorption spectrometry (GF-AAS) on acidified samples. The detection limits for GF-AAS analysis was 0.2 μM, and the precision was 0.4 μM (2-SD) for both metals. Dissolved sulfate concentrations were determined using ion chromatography.

Frozen wet sediments were analyzed for solid-Fe phases. Labile Fe (Fe_{HCl}) was extracted using cold 0.5 M HCl for 1 h. This method extracts amorphous Fe(III)-oxides, FeS, non-S particulate Fe(II), some silicate Fe (e.g., chlorite), but not crystalline Fe such as goethite, hematite, magnetite and pyrite (Kostka and Luther, 1994). We note that this method only extracts highly reactive Fe minerals and therefore underestimates the total reactive Fe concentrations relative to the commonly applied dithionite and 1 min boiling HCl methods (Berner, 1970; Raiswell et al., 1988; Canfield, 1989; Raiswell et al., 1994). Iron concentrations were measured spectrophotometrically using the *Ferrozine* method of Stookey (1970). Ferrous Fe in the HCl extract was determined after adding *Ferrozine* reagent (0.02% *Ferrozine* in 50 mM HEPES buffer, pH 7) to a small aliquot of the sample. Total Fe for the HCl and all other sediment extractions was determined using *Ferrozine* reagent, in the presence of a reducing agent (1% hydroxalamine hydrochloride). The concentration of ferric Fe in the HCl-extractable Fe was calculated by subtraction of Fe(II) from total HCl–Fe.

Solid phase components of magnetite, pyrite and silicate were separated using standard methods. Magnetite was separated with a strong magnet, using a modified version of the method of Canfield and Berner (1987). The mineral separates were dissolved in 6 M HCl, and total magnetite Fe (Fe_{Mt}) was determined as above. Pyrite–Fe (Fe_{Py}) was determined using the sequential extraction method of Huerta-Diaz and Morse (1990). Following HCl treatment, the residual sediments were treated in 10 M HF for 16 h to dissolve any silicate Fe, and this fraction was not analyzed further. The only significant Fe phase in the residual sediments, following HCl and HF treatment, is pyrite (Huerta-Diaz and Morse, 1990), which was dissolved in concentrated HNO_3 over 2 h. Total solid phase Fe (Fe_{tot}) was determined in dried sediments that were heated at 850 °C for 6 h, followed by total digestion in a mixture of HF and HNO_3. Sediment Fe concentrations are reported as dwt.%. ^{210}Pb contents in the SBB sediments were measured by gamma counting (Gilmore and Hemingway, 1995) and corrected for background (supported) ^{210}Pb by subtracting the activity of ^{226}Ra. ^{210}Pb data were collected on dried sediments from a parallel multicore from the same deployment. All other concentration and isotope data were obtained on samples from the same cores.

3.2. Iron isotope analysis

Iron isotope analysis was performed on a GV Instruments *IsoProbe* multi-collector inductively coupled plasma mass-spectrometer (MC-ICP-MS) at the University of Wisconsin, Madison. A high ratio of major ions (esp. Ca and Mg) to Fe in marine porewaters poses a particular challenge because of the potential for isobaric interference during Fe isotope analysis (e.g., $^{40}Ca^{16}OH$ on ^{57}Fe), as well as possible matrix effects, which can adversely impact accuracy of Fe isotope measurements (Albarède and Beard, 2004). For the initial purification step of porewater samples we adopted a procedure that uses a 500 μl volume of 8-hydroxiquinoline (8-HQ) resin, which is commonly used for pre-concentration and purification of metals from seawater (Dierssen et al., 2001). Pre-concentrated samples were further processed through standard anion-exchange chromatography two to three times (Beard et al., 2003a). To test the porewater purification method for analytical bias that might be introduced during chemical processing, we prepared a synthetic porewater sample by adding a small amount ($\sim$1 μg Fe) of High Purity Standard (UW-HPS Fe) or IRMM-014 Fe to 2 ml of trace-metal-free seawater. The ratio of Fe to major seawater ions in the synthetic porewaters matched the lowest Fe to seawater-matrix ratio in the porewater samples. The isotope

Table 2
Fe isotope composition of artificial porewater samples

Sample[a]	δ^{56}Fe	2-SE	δ^{57}Fe	2-SE
UW-HPS dope 1	0.47	±0.08	0.74	±0.04
UW-HPS dope 2	0.32	±0.05	0.54	±0.03
UW-HPS dope 3	0.43	±0.05	0.63	±0.04
UW-HPS dope 4	0.53	±0.04	0.87	±0.04
UW-HPS nominal[b]	0.49	±0.05	0.74	±0.07
IRMM-014 dope	−0.06	±0.04	−0.12	±0.03
IRMM-014 nominal[b]	−0.09	±0.05	−0.11	±0.07

[a] To test for bias introduced during sample processing, a small aliquot of ultra-pure standard UW-HPS Fe or IRMM-014 was added to trace-metal free seawater.
[b] Isotope composition of UW-HPS Fe based on 52 analysis and IRMM-014 based on 54 analysis at UW-Madison.

composition of the synthetic porewater, following chemical purification, was analytically indistinguishable from the pure, unprocessed Fe standards (Table 2). Sediment extracts were processed through anion-exchange columns two to three times. The recovery of Fe following chemical processing was monitored for each sample, and only samples that had a yield of $\geqslant$95% were used for Fe isotope analysis.

Instrumental mass-bias was corrected using a standard bracketing approach. Samples were introduced into the mass-spectrometer as 200 or 400 ppb Fe solutions. Data are reported using standard δ notation in units of per mil (parts per 10^3 or ‰) for $^{56}Fe/^{54}Fe$ ratios

$$\delta^{56}\mathrm{Fe} = \left(\frac{^{56}\mathrm{Fe}/^{54}\mathrm{Fe}_{\mathrm{SAMPLE}}}{^{56}\mathrm{Fe}/^{54}\mathrm{Fe}_{\mathrm{IG\ RXS}}} - 1\right) \times 10^3, \quad (1)$$

where $^{56}Fe/^{54}Fe_{IG\ RXS}$ represents the average isotopic compositions of terrestrial igneous rocks, which have a δ^{56}Fe of 0.00 ± 0.05‰ (Beard et al., 2003a). On this scale, the δ^{56}Fe value of the IRMM-14 standard is −0.09‰ (Beard et al., 2003a). Data reported for $^{57}Fe/^{54}Fe$ ratios may be converted to δ^{56}Fe values by multiplying the δ^{57}Fe value by ~0.667. The average external 1-SD reproducibility of the analysis is ±0.05‰ for δ^{56}Fe and ±0.07‰ for δ^{57}Fe, as determined by duplicate analysis of 27 of the 84 samples analyzed in this study via re-processing of different sample aliquots through chemistry. This precision is identical to the long-term (several years) external precision obtained for ultra-pure Fe metal standards (Beard et al., 2003a).

4. Results

4.1. Porewater and solid phase concentrations

Ammonia concentrations in pore fluids at both stations increase with increasing depth, indicating significant organic carbon cycling at our study sites. Concentrations are markedly higher at the MC station, reaching maximum values of 2.0 mM compared to only 0.3 mM at SBB (Table 3, Fig. 1). Ammonia concentrations in the slope sediments from the SBB compare well with published values of 0.2 mM (Sholkovitz, 1973). Similar contrasts are seen in dissolved sulfate concentrations, where at the MC station they decrease progressively from a maximum value of 25.2 mM near the surface to 3.4 mM at the base of the gravity core (152.5 cm; Table 3, Fig. 1). Sulfate concentrations at the SBB site decrease slightly with depth. The absence of significant sulfate depletion in SBB sediments is in good agreement with data of Sholkovitz (1973), who also did not observe a decrease in sulfate concentrations in slope sediments of the SBB. Total sulfide contents in the gravity core were below the detection limit in the MC sediments but increase in concentration below ~50 cm depth in the SBB sediments (Fig. 1). Although it is surprising that there is a significant dissolved sulfate gradient but no sulfide gradient in the MC sediments, the exceptionally high concentration of dissolved Fe throughout the MC core indicates that dissolved sulfide at this site should be consumed during reduction of Fe(III)-oxides or quantitatively titrated by dissolved Fe $(II)_{aq}$. These $Fe(II)_{aq}$ concentrations are higher than any previously reported porewater $Fe(II)_{aq}$ contents for this area (Shaw et al., 1990; Reimers et al., 1996; McManus et al., 1997). High pore fluid $Fe(II)_{aq}$ contents at the MC site are consistent with the high benthic Fe fluxes that were predicted and measured in Monterey Bay sediments (Berelson et al., 2003; Elrod et al., 2004). A sharp peak in $Fe(II)_{aq}$ is observed in the gravity core and is mimicked in the $Mn(II)_{aq}$ concentrations for the same core (data not shown), but similar peaks are not present in the porewaters from the multi-core. The two cores from MC were recovered from approximately the same station; however, this is a dynamic region in terms of sediment transport, and it is possible that the two sites have different quantities of reactive Fe and Mn but similar carbon supply rates. In comparison, porewater $Fe(II)_{aq}$ concentrations in the sediments from the SBB site are markedly lower (maximum 185 μM; Table 3, Fig. 1). Both stations have elevated $Fe(II)_{aq}$ concentrations within the top 1 cm of the sediments.

Solid phase Fe_{tot} concentrations are similar at both sites, and the average Fe_{tot} is 5.0 ± 0.8 dwt.% and 4.7 ± 0.2 dwt.% at stations MC and SBB, respectively (Table 3, Fig. 2). Highly reactive Fe (Fe_{HR}) is defined as the fraction of initial Fe that is available for, or has already undergone, reductive dissolution during early diagenesis. The concentration of Fe_{HR} is calculated as

$$[\mathrm{Fe_{HR}}] = [\mathrm{Fe(II)_{aq}}] + [\mathrm{Fe(II)_{HCl}}] + [\mathrm{Fe(III)_{HCl}}] + [\mathrm{Fe_{Mt}}] + [\mathrm{Fe_{Py}}] \quad (2)$$

and comprises an average of 13.0 ± 1.7% of Fe_{tot} at MC and 14.8 ± 3.4% of Fe_{tot} at SBB (Table 3, Fig. 2). Magnetite is markedly higher at the MC station, comprising an average of 5.5% of the Fe_{HR} fraction compared to only 1% at the SBB locality (Table 3, Fig. 2). Pyrite concentrations in the MC sediments are low, averaging 5.3% of Fe_{HR}, and are relatively constant downwards, whereas at the SBB site, pyrite

Table 3
Porewater and solid phase concentrations for major ions and Fe-bearing minerals

Sample ID	Depth (cm)	Porewater concentrations				Solid phase concentrations				
		Ammonia (mM)	Sulfate (mM)	ΣH_2S (μM)	$Fe(II)_{aq}$ (μM)	Fe_{tot} (dwt.%)	Fe_{HCl} (dwt.%)	$Fe(II)_{HCl}/Fe_{HCl}$	Fe_{Py} (dwt.%)	Fe_{Mt} (dwt.%)
Monterey Canyon										
MC-MC#1	0.5	0.10			**150.0**	**5.00**	**0.53**	0.44	**0.02**	0.03
MC-MC#2	1.5	0.17			795.9					
MC-MC#3	2.5	0.20								
MC-MC#4	3.5	0.22			**892.6**	**4.87**	**0.53**	0.58	**0.03**	0.01
MC-MC#5	4.5	0.20			685.3					
MC-MC#6	5.5	0.21			**655.3**	**5.50**	**0.61**	0.53	**0.03**	0.01
MC-MC#7	7.3	0.16			595.0					
MC-MC#8	9.8	0.17			**539.0**	**5.42**	**0.50**	0.69	**0.03**	0.04
MC-MC#9	12.3	0.26			283.1					
MC-MC#10	14.8	0.53			**352.1**	**3.09**	**0.39**	0.86	**0.04**	0.08
MC-MC#11	17.3	0.78			536.4					
MC-MC#12	19.8	0.85			**266.9**	**5.69**	**0.69**	0.66	**0.05**	0.02
MC-MC#13	22.3	0.92			108.5					
MC-MC#14	24.8	0.90			**277.3**	**5.62**	**0.69**	0.66	**0.04**	0.04
MC-MC#15	27.3	0.84			416.5					
MC-MC#16	29.8	0.91			**465.1**	**5.81**	**0.68**	0.58	**0.04**	0.02
MC-MC#17	32.3	0.95			**493.2**	**5.02**	**0.58**	0.65	**0.04**	0.05
MC-MC#18	34.8	1.04								
MC-MC#19	37.3	1.15								
MC-MC#20	39.8	1.22			**88.3**	**5.11**	**0.73**	0.58	**0.04**	0.03
MC-MC#21	42.3	1.28			229.5					
MC-MC#22	44.8	1.34			**257.8**	**5.08**	**0.59**	0.88	**0.03**	0.03
MC-MC#23	47.3	1.40			131.2					
MC-MC#24	49.8	1.41			**257.8**	**4.14**	**0.43**	0.66	**0.03**	0.04
MC-GC#25	5.5	0.49	25.2	<1	128.8					
MC-GC#26	14.5	0.63	24.1	1.1	338.0					
MC-GC#27	25.5	0.81	23.1	1.3	835.2					
MC-GC#28	35.5	1.12	19.8	<1	1935.9					
MC-GC#29	45.5	1.42	16.4	<1	730.3					
MC-GC#30	55.5	1.43	14.9	<1	24.0					
MC-GC#31	65.5	1.36	13.8	<1	15.1					
MC-GC#32	75.5	1.31	13.9	<1	60.4					
MC-GC#33	85.5	1.25	14.3	1.0	85.8					
MC-GC#34	95.5	1.25	13.8	<1	275.3					
MC-GC#35	105.5	1.29	12.8	1.0	432.0					
MC-GC#36	115.5	1.51	9.1	<1	209.1					
MC-GC#37	125.5	1.61	6.9	<1	55.2					
MC-GC#38	135.5	1.90	5.4	1.2						
MC-GC#39	145.5	1.99	4.1	1.1	258.6					
MC-GC#40	152.5	2.06	3.4	1.1	164.9					
Santa Barbara basin										
SBB-MC#101	0.5	0.05	28.4		**92.6**	**4.80**	**0.70**	0.36	**0.05**	0.01
SBB-MC#102	1.5	0.05	28.6		185.2					
SBB-MC#103	2.5	0.07	28.2		**163.5**	**4.69**	**0.28**	0.68	**0.08**	0.00
SBB-MC#104	3.5	0.09	27.7		157.7					
SBB-MC#105	4.5	0.10	27.8		**121.0**	**4.49**	**0.41**	0.63	**0.14**	0.01
SBB-MC#106	5.5	0.22	27.8		112.5					
SBB-MC#107	7.3	0.13	28.1		**110.6**	**4.90**	**0.47**	0.91	**0.26**	0.00
SBB-MC#108	9.8	0.14	28.1		32.7					
SBB-MC#109	12.3	0.15	27.2		**37.9**	**4.79**	**0.41**	0.90	**0.42**	0.01
SBB-MC#110	14.8	0.14	27.9		24.1					
SBB-MC#111	17.3	0.15	27.6		**24.3**	**4.46**	**0.30**	0.84	**0.29**	0.01
SBB-MC#112	19.8	0.18	27.0		7.6					
SBB-MC#113	22.3	0.19	26.9		**24.3**	**4.90**	**0.37**	0.96	**0.34**	0.01
SBB-MC#114	24.8	0.17	27.0		23.2					
SBB-MC#115	27.3	0.20	26.8		**30.4**	**4.95**	**0.38**	0.89	**0.50**	0.01
SBB-MC#116	29.8	0.22	26.3		28.1					
SBB-MC#117	32.3	0.23	26.5		**16.3**	**4.30**	**0.37**	0.99	**0.44**	0.01
SBB-GC#149	15.5	0.19	27.7	<1	17.5					
SBB-GC#150	25.5		26.3	<1	13.8					

Table 3 (*continued*)

Sample ID	Depth (cm)	Porewater concentrations				Solid phase concentrations				
		Ammonia (mM)	Sulfate (mM)	ΣH_2S (μM)	$Fe(II)_{aq}$ (μM)	Fe_{tot} (dwt.%)	Fe_{HCl} (dwt.%)	$Fe(II)_{HCl}/Fe_{HCl}$	Fe_{Py} (dwt.%)	Fe_{Mt} (dwt.%)
SBB-GC#151	35.5	0.26	26.2	<1	9.0					
SBB-GC#152	45.5	0.26	26.8	<1	4.7					
SBB-GC#153	55.5	0.27	26.4	<1	1.7					
SBB-GC#154	65.5				0.4					
SBB-GC#155	75.5	0.28	26.3	34.8	0.6					
SBB-GC#156	85.5		26.5	73.4	0.4					
SBB-GC#157	95.5	0.29	26.3		0.5					
SBB-GC#158	105.5	0.27	26.1							
SBB-GC#159	115.5	0.26	26.9		0.9					
SBB-GC#160	125.5		26.3	188.5	0.7					
SBB-GC#161	135.5		26.5	71.6	0.6					
SBB-GC#162	150.0	0.22	26.5		0.3					
SBB-GC#163	162.0	0.19	26.7	72.5	0.4					

Bold numbers indicate samples that were analyzed for Fe isotope composition. Speciation of dissolved Fe was not determined, but Fe(III) is assumed to be negligible because of its the low solubility at ambient conditions.

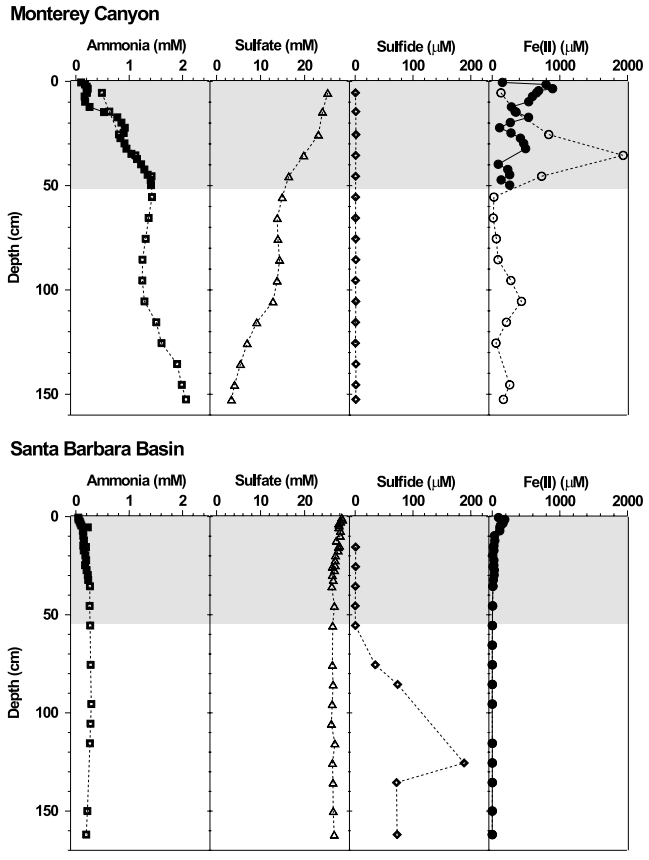

Fig. 1. Porewater profiles of ammonia, sulfate, hydrogen sulfide, and aqueous Fe(II) for the two sites on the California continental margin. For $Fe(II)_{aq}$ and ammonia, filled symbols are for porewaters from the multi-core, and empty symbols are for the gravity core. Only samples from the multi-core were analysed for Fe isotope compositions (shaded area). Ammonia concentrations indicate that microbial carbon respiration is much higher at Monterey Canyon (MC) relative to Santa Barbara basin (SBB). Sulfate is consumed during bacterial sulfate reduction (BSR), but high-$Fe(II)_{aq}$ concentrations in the MC sediments probably prevent build-up of sulfide in the porewaters. The large peak in porewater Fe(II) between 30 and 40 cm depth in the MC sediments is attributed to a sediment disturbance, such as a turbidite.

contents increase from 6.4% of Fe_{HR} near the surface to 53.8% of Fe_{HR} at the base of the multi-core (32 cm depth; Fig. 2). The markedly higher iron sulfide contents at the SBB locality correlates with the much lower $Fe(II)_{aq}$ concentrations at this locality relative to those observed at the MC site. Fe_{HCl} is the dominant fraction of the highly reactive Fe pool, comprising an average of 89.3% of Fe_{HR} at MC and 60.5% of Fe_{HR} at SBB (Fig. 2). The concentration of $Fe(III)_{HCl}$ is relatively constant with depth in MC sediments but decreases to 1% of HCl-extractable Fe at SBB. The proportion of HCl-extractable Fe that is ferrous averages $64.7 \pm 12.6\%$ at MC and $79.8 \pm 20.2\%$ at SBB. Most of the $Fe(II)_{HCl}$ is believed to be bound by S^{2-}, and for convenience we will refer to this fraction as FeS. This interpretation is consistent with the sediment's dark brown to black color and the strong sulfidic smell that developed during HCl extraction of sediments from both sites, although we did not measure reduced or total solid phase sulfur concentrations directly. It should be noted, however, that a significant proportion of authigenic, non-sulfidic, particulate Fe(II) is commonly observed in sulfidic sediments (Thamdrup et al., 1994; Thamdrup and Canfield, 1996), comprising as much as 30% of the total reactive Fe (Thamdrup et al., 1994). Poulton (2003) has confirmed the presence of this non-S Fe(II) experimentally, and Poulton et al. (2004) suggest that this pool represents a non-dissolved Fe(II) phase that remains associated with the oxide surface.

Excess ^{210}Pb concentrations in SBB sediments decrease progressively until they reach relatively constant values at ~30 cm depth (Table 4, Fig. 3). A sedimentation rate of 2.5 mm yr^{-1} was calculated for the surface 30 cm depth interval assuming uniform sedimentation and absence of significant bioturbation.

4.2. Fe isotope compositions

Sediments and porewaters from the multi-cores were analysed for their Fe isotope compositions (Table 5,

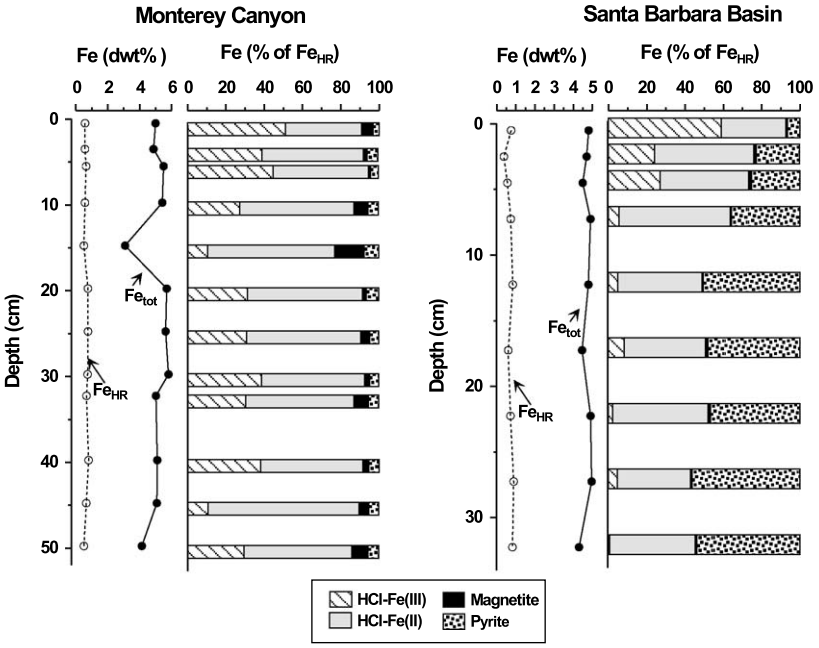

Fig. 2. Partitioning of solid Fe phases as a proportion of the highly reactive Fe (Fe_{HR}) pool. Note that on this scale, $Fe(II)_{aq}$ contributes negligibly to the highly reactive Fe pool and so is not plotted. Line graphs show the concentrations of Fe_{tot} and Fe_{HR}. Bioturbation, bioirrigation, and sediment slumping at the MC site cause a continuous re-charge of oxidants. The presence of highly reactive Fe(III) and magnetite throughout this core indicates that DIR is an important pathway for carbon oxidation at this site. In contrast, BSR is the dominant pathway of organic matter oxidation below ~10 cm depth in the SBB sediments, as indicated by the absence of highly reactive Fe(III) and the significant quantity of pyrite.

Fig. 4). For the solid phase, Fe isotope compositions were determined for the total solid (Fe_{tot}), the HCl-extractable component (Fe_{HCl}) and the pyrite component (Fe_{Py}). The $\delta^{56}Fe$ values of these components span a range nearly equal to that observed for all terrestrial samples, from $-3.0‰$ to $+0.4‰$. The range in $\delta^{56}Fe$ values for the solid phase components is not an artifact of the extraction procedure. Partial dissolution of many solid phases by HCl, HNO_3 and HF has been shown to produce no isotopic fractionation if they dissolve congruently (Skulan et al., 2002; Beard and Johnson, 2004; S. Severmann unpublished results). Further, Brantley et al. (2004) have shown that extractions using citrate–dithionite, another standard method of subsampling solid phase components, do not produce isotopic fractionations, suggesting that the reactive Fe mineral phases dissolve congruently using these extraction procedures.

The $\delta^{56}Fe$ values of Fe_{tot} cluster about the average for igneous rocks at $\delta^{56}Fe = 0‰$ (Fig. 4; Beard et al., 2003a). In addition, the $\delta^{56}Fe$ values for Fe_{tot} from the MC and SBB sites are in close agreement with previously reported data for total digests of modern marine sediments and suspended river particulates, which have $\delta^{56}Fe = +0.04 \pm 0.07‰$ and $-0.01 \pm 0.06‰$, respectively (Beard et al., 2003b; Fantle and DePaolo, 2004). In contrast to the isotopic homogeneity of Fe_{tot}, $Fe(II)_{aq}$ varies the greatest in Fe isotope compositions, where the $\delta^{56}Fe$ values range from $-3.0‰$ to $+0.4‰$. The $\delta^{56}Fe$ values for $Fe(II)_{aq}$ from the MC locality porewaters are all negative ($<-0.6‰$), and the lowest $\delta^{56}Fe$ values correlate with the lowest $Fe(II)_{aq}$ contents (Fig. 4). In contrast, at the SBB locality, $\delta^{56}Fe$ values change from $<0‰$ near the surface to $>0‰$ with increasing depth; with the exception of one sample, the $\delta^{56}Fe$ compositions of $Fe(II)_{aq}$ at the SBB locality closely track those of Fe_{HCl} below ~10 cm (Fig. 4). Compared to the wide range in $\delta^{56}Fe$ values for $Fe(II)_{aq}$ and Fe_{HCl}, the Fe isotope composition of the pyrite fraction is relatively constant at both stations, where the average $\delta^{56}Fe$ value is $-0.8 \pm 0.2‰$.

The isotopic composition of Fe_{HR} is calculated from isotopic mass balance

$$\delta^{56}Fe_{HR} = \delta^{56}Fe_{Fe(II)_{aq}} \times X_{Fe(II)_{aq}} + \delta^{56}Fe_{HCl} \times X_{HCl} + \delta^{56}Fe_{Py} \times X_{Py}, \quad (3)$$

where X denotes the mole fraction of each component. Magnetite is omitted from this calculation because no isotope compositions were obtained for the Fe_{Mt} fraction. However, because magnetite is generally <8% of Fe_{HR}, the isotope composition of magnetite would have to be several per mil different from the bulk Fe to significantly affect the calculated Fe_{HR} isotope composition, which would be inconsistent with experimental work that indicated a $-1.3‰$ fractionation between $Fe(II)_{aq}$ and magnetite (Johnson et al., 2005). The average $\delta^{56}Fe$ value of Fe_{HR} from both stations is similar at $-0.40 \pm 0.13‰$, which is significantly lower than the average $\delta^{56}Fe$ value of Fe_{tot}. Notably, the Fe isotope composition for Fe_{HR} trends to lower $\delta^{56}Fe$ values upward in the upper 10 cm of the MC core, where the lowest $\delta^{56}Fe$ values occur near the surface. By simple mass balance we derive an isotope composition

Table 4
Excess ^{210}Pb and supported ^{226}Ra concentrations for Santa Barbara basin sediments

Depth (cm)	Excess ^{210}Pb (dpm/g)	^{210}Pb error (dpm/g)	Supported ^{226}Ra (dpm/g)	^{226}Ra error (dpm/g)
0.25	29.9	1.5	2.5	0.3
0.75	58.8	1.7	3.9	0.2
1.25	49.8	1.6	3.7	0.2
1.75	45.8	1.3	3.4	0.2
2.25	41.8	1.0	3.0	0.2
2.75	41.8	1.1	3.3	0.2
3.25	41.9	1.2	3.5	0.2
3.75	40.8	1.0	3.4	0.1
4.25	39.6	0.9	3.4	0.1
4.75	38.8	0.9	3.5	0.1
5.25	38.0	0.9	3.6	0.1
5.75	34.6	1.0	3.5	0.1
6.25	31.2	1.1	3.3	0.1
6.75	29.7	1.0	3.3	0.1
7.25	28.1	0.9	3.2	0.1
7.75	27.2	0.9	3.3	0.1
8.25	26.2	0.8	3.3	0.1
8.75	26.8	0.9	3.5	0.1
9.25	27.3	0.9	3.7	0.2
9.75	23.3	1.0	3.4	0.2
10.50	18.4	0.7	3.3	0.1
11.50	15.2	0.6	3.5	0.1
12.50	12.0	0.5	3.5	0.1
13.50	9.4	0.4	3.4	0.1
14.50	6.7	0.3	3.3	0.1
16.50	5.5	0.3	3.0	0.1
18.50	4.3	0.4	2.8	0.1
21.00	3.4	0.3	3.0	0.1
25.00	2.5	0.3	3.1	0.1
29.00	1.3	0.3	3.2	0.1
33.00	0.2	0.3	3.3	0.1
37.00	0.2	0.3	3.4	0.1
41.00	0.3	0.3	3.4	0.1

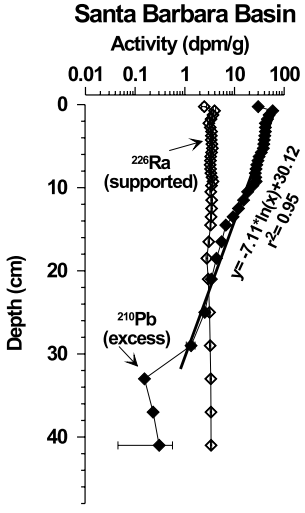

Fig. 3. Lithogenous (supported) ^{226}Ra and excess ^{210}Pb profiles for the surface sediments from SBB, suggesting that bioturbation is absent at this site. The sedimentation rate calculated from this profile is 2.5 mm yr^{-1}, consistent with previous estimates for the SBB (Koide et al., 1972; Zheng et al., 2000). Data from Table 4. Error bars are equal to or smaller than the size of the symbol except where displayed.

for the non-reactive Fe pool, which we define as $Fe_{residual}$ (Fig. 4) and which has a δ^{56}Fe value of $+0.07 \pm 0.06‰$; $Fe_{residual}$ is likely to include a mixture of primary and secondary silicate minerals, and its isotopic composition overlaps the average for igneous rocks.

5. Discussion

5.1. Major pathways of organic matter oxidation and Fe transformations

One significant distinction between the two sites is the nature of Fe cycling that has occurred. Contrasts in the solid phase proportions of the reactive Fe pool between the two sites, such as the relatively high proportion of $Fe(II)_{aq}$ and HCl-extractable reactive Fe(II) and Fe(III) contents in the solid phase at the MC site, and the high proportion of insoluble pyrite in the SBB site (Fig. 2), suggests that Fe cycling was more active at the MC locality as compared to the SBB site. This contrast is reflected in the Fe isotope compositions between the two sites (Fig. 4). If we assume that the difference in the ammonia contents of the pore fluids is driven by differences in the amount of carbon respired, the markedly higher ammonia levels at the MC site (Fig. 1) suggest higher levels of microbial reduction and total carbon respiration. This interpretation would require that, despite similar carbon rain rates for the two localities (Thunell et al., 1995; Pilskaln et al., 1996), MC sediments must have a lower carbon burial efficiency. This contention is consistent with the observation of high organic carbon contents in the SBB compared to the MC site.

The irregular shape of the $Fe(II)_{aq}$ profile in the MC sediments (Fig. 1) is characteristic of bioturbated sediments (e.g., Aller et al., 1986; Canfield and Des Marais, 1993). ^{210}Pb data from the Monterey Bay suggest a well-mixed (bioturbated) upper 10 cm and an average sedimentation rate of 2.5 mm yr^{-1} (Berelson et al., 2003). Further, Berelson et al. (2003) demonstrate that advective processes (bioirrigation) enhance diffusive transport in these sediments by a factor of 2.5–11. Sediments of the SBB, in contrast, do not appear to undergo significant bioirrigation (Fig. 3), consistent with anoxic conditions within the upper few millimeters, as well as the presence of finely laminated sediments within the basin (Bruland et al., 1981; Kennett and Ingram, 1995; Reimers et al., 1996; Behl and Kennett, 1999). The sediment accumulation rate for our particular SBB core of 2.5 mm yr^{-1} is similar to a previous estimate for the basin of 4 mm yr^{-1} (Koide et al., 1972; Zheng et al., 2000). Although we did not measure oxygen, nitrate and Mn-oxides directly, we assume that these oxidants are exhausted within the surface few millimeters of the SBB sediments (Reimers et al., 1996), consistent with accumulation of $Fe(II)_{aq}$ in the upper 1 cm interval of the multi-core. In the MC sediments it is likely that bioturbative mixing resupplies oxidants such as nitrate and Mn-oxides down to a few centimeters depth, but porewater $Fe(II)_{aq}$ concentrations >150 μM in the surface interval indicate that carbon

Table 5
Fe isotope compositions of porewater Fe, particulate total Fe, HCl-extractable Fe and pyrite

Sample	Depth (cm)	Aliquot[a]	Individual analysis				Grand mean	
			δ^{56}Fe	2-SE	δ^{57}Fe	2-SE	δ^{56}Fe	1-SD[b]
Sediment total digest								
MC-MC#1-td	0.50	1	−0.09	±0.03	−0.14	±0.03	−0.09	±0.00
		1	−0.09	±0.03	−0.02	±0.03		
MC-MC#4-td	3.50	1	−0.07	±0.04	−0.03	±0.03	−0.07	±0.04
MC-MC#6-td	5.50	1	−0.03	±0.04	0.04	±0.04	−0.03	±0.04
MC-MC#8-td	9.75	1	0.08	±0.07	0.08	±0.03	0.08	±0.07
MC-MC#10-td	14.75	1	0.00	±0.04	0.00	±0.04	0.00	±0.04
MC-MC#12-td	19.75	1	0.02	±0.04	0.05	±0.03	−0.01	±0.03
		1	−0.03	±0.04	−0.01	±0.05		
MC-MC#14-td	24.75	1	−0.02	±0.04	−0.07	±0.03	−0.02	±0.04
MC-MC#16-td	29.75	1	0.02	±0.06	−0.01	±0.04	0.02	±0.06
MC-MC#17-td	32.25	1	0.08	±0.03	0.05	±0.03	0.03	±0.07
		1	−0.02	±0.03	0.01	±0.03	0.03	±0.06
MC-MC#20-td	39.75	1	0.10	±0.03	0.12	±0.03	0.10	±0.03
MC-MC#22-td	44.75	1	0.02	±0.03	0.13	±0.03	0.02	±0.03
MC-MC#24-td	49.75	1	0.01	±0.03	0.01	±0.04	0.01	±0.03
SBB-MC#101-td	0.5	1	−0.09	±0.03	−0.14	±0.04	−0.09	±0.03
SBB-MC#103-td	2.5	1	−0.02	±0.04	−0.01	±0.03	−0.03	±0.01
		2	−0.04	±0.04	0.01	±0.03		
SBB-MC#105-td	4.5	1	0.00	±0.03	0.06	±0.03	0.00	±0.03
SBB-MC#107-td	7.25	1	0.07	±0.03	0.08	±0.03	0.07	±0.03
SBB-MC#109-td	12.25	1	0.02	±0.03	0.06	±0.03	0.01	±0.01
		1	0.00	±0.03	−0.01	±0.03		
SBB-MC#111-td	17.25	1	0.05	±0.03	0.09	±0.03	0.05	±0.03
SBB-MC#113-td	22.25	1	0.00	±0.04	0.08	±0.03	0.01	±0.02
		2	0.03	±0.04	0.16	±0.03		
SBB-MC#115-td	27.25	1	0.04	±0.04	0.06	±0.03	0.04	±0.02
		1	0.02	±0.03	0.03	±0.03		
		2	0.06	±0.03	0.08	±0.03		
SBB-MC#117-td	32.25	1	−0.05	±0.07	−0.05	±0.04	−0.02	±0.05
		1	0.01	±0.03	0.04	±0.03		
Sediment HCl extractions								
MC-MC#1-HCl	0.50	1	−0.88	±0.03	−1.31	±0.03	−0.88	±0.03
MC-MC#4-HCl	3.50	1	−0.60	±0.04	−0.88	±0.04	−0.57	±0.05
		1	−0.58	±0.03	−0.90	±0.03		
		2	−0.51	±0.03	−0.79	±0.03		
MC-MC#6-HCl	5.50	1	−0.49	±0.04	−0.57	±0.03	−0.51	±0.02
		1	−0.52	±0.04	−0.67	±0.02		
MC-MC#8-HCl	9.75	1	−0.37	±0.03	−0.59	±0.04	−0.32	±0.06
		1	−0.28	±0.03	−0.33	±0.03		
MC-MC#10-HCl	14.75	1	−0.43	±0.04	−0.62	±0.03	−0.40	±0.04
		1	−0.36	±0.03	−0.55	±0.03		
		2	−0.43	±0.03	−0.59	±0.03		
		2	−0.36	±0.04	−0.46	±0.03		
MC-MC#12-HCl	19.75	1	−0.18	±0.04	−0.28	±0.03	−0.18	±0.04
MC-MC#14-HCl	24.75	1	−0.42	±0.02	−0.59	±0.02	−0.42	±0.02
MC-MC#16-HCl	29.75	1	−0.39	±0.03	−0.54	±0.02	−0.39	±0.00
		2	−0.39	±0.04	−0.58	±0.03		
MC-MC#17-HCl	32.25	1	−0.53	±0.02	−0.58	±0.02	−0.53	±0.02
MC-MC#20-HCl	39.75	1	−0.41	±0.02	−0.60	±0.02	−0.39	±0.02
		2	−0.38	±0.04	−0.55	±0.03		
MC-MC#22-HCl	44.75	1	−0.45	±0.03	−0.64	±0.03	−0.40	±0.07
		2	−0.35	±0.04	−0.45	±0.04		
MC-MC#24-HCl	49.75	1	−0.24	±0.02	−0.34	±0.03	−0.32	±0.12
		2	−0.41	±0.03	−0.60	±0.03		
SBB-MC#101-HCl	0.5	1	−0.29	±0.03	−0.44	±0.02	−0.33	±0.06
		2	−0.37	±0.04	−0.51	±0.03		
SBB-MC#103-HCl	2.5	1	−0.13	±0.02	0.16	±0.03	−0.13	±0.02
SBB-MC#105-HCl	4.5	1	−0.26	±0.03	±0.23	±0.03	−0.26	±0.03
SBB-MC#107-HCl	7.25	1	−0.06	±0.10	0.01	±0.04	−0.03	±0.02
		1	−0.02	±0.03	−0.10	±0.03		
		1	−0.01	±0.03	0.00	±0.03		

Table 5 (*continued*)

Sample	Depth (cm)	Aliquot[a]	Individual analysis				Grand mean	
			δ^{56}Fe	2-SE	δ^{57}Fe	2-SE	δ^{56}Fe	1-SD[b]
		2	−0.04	±0.04	−0.03	±0.03		
SBB-MC#109-HCl	12.25	1	0.15	±0.04	0.20	±0.04	0.15	±0.04
SBB-MC#111-HCl	17.25	1	0.26	±0.05	0.37	±0.03	0.25	±0.00
		2	0.25	±0.03	0.38	±0.03		
SBB-MC#113-HCl	22.25	1	0.44	±0.04	0.65	±0.03	0.44	±0.04
SBB-MC#115-HCl	27.25	1	0.19	±0.02	0.28	±0.02	0.19	±0.02
SBB-MC#117-HCl	32.25	1	0.30	±0.04	0.47	±0.04	0.35	±0.06
		1	0.41	±0.04	0.64	±0.04		
		2	0.36	±0.04	0.52	±0.04		
Pyrite fraction								
MC-MC#1-py	0.50	1	−0.50	±0.04	−0.69	±0.04	−0.49	±0.02
		2	−0.47	±0.04	−0.66	±0.03		
MC-MC#4-py	3.50	1	−0.73	±0.04	−1.04	±0.03	−0.71	±0.02
		1	−0.69	±0.03	−1.08	±0.03		
		1	−0.71	±0.05	−1.03	±0.04		
MC-MC#6-py	5.50	1	−0.49	±0.04	−0.76	±0.03	−0.49	±0.04
MC-MC#8-py	9.75	1	−0.86	±0.05	−1.31	±0.04	−0.86	±0.05
MC-MC#10-py	14.75	1	−0.85	±0.03	−1.21	±0.03	−0.85	±0.03
MC-MC#12-py	19.75	1	−0.67	±0.05	−0.88	±0.04	−0.71	±0.06
		2	−0.76	±0.05	−1.05	±0.05		
MC-MC#14-py	24.75	1	−0.70	±0.05	−1.00	±0.04	−0.70	±0.01
		1	−0.69	±0.03	−1.03	±0.02		
MC-MC#16-py	29.75	1	−0.80	±0.04	−1.24	±0.03	−0.80	±0.04
MC-MC#17-py	32.25	1	−0.79	±0.03	−1.16	±0.03	−0.74	±0.07
		2	−0.69	±0.05	−0.92	±0.02		
MC-MC#20-py	39.75	1	−0.83	±0.04	−1.18	±0.04	−0.83	±0.04
MC-MC#22-py	44.75	1	−0.64	±0.19	−1.02	±0.25	−0.71	±0.07
		1	−0.78	±0.05	−1.19	±0.04		
		1	−0.71	±0.04	−0.99	±0.03		
MC-MC#24-py	49.75	1	−0.74	±0.05	−1.03	±0.04	−0.69	±0.04
		1	−0.66	±0.03	−0.95	±0.02		
		2	−0.68	±0.06	−0.84	±0.03		
SBB-MC#101-py	0.5	1	−0.64	±0.04	−0.93	±0.03	−0.64	±0.04
SBB-MC#103-py	2.5	1	−0.72	±0.04	−0.96	±0.04	−0.78	±0.09
		1	−0.84	±0.05	−1.18	±0.03		
SBB-MC#105-py	4.5	1	−0.77	±0.02	−1.13	±0.03	−0.76	±0.03
		2	−0.74	±0.06	−1.00	±0.04		
SBB-MC#107-py	7.25	1	−0.74	±0.04	−1.12	±0.02	−0.74	±0.04
SBB-MC#109-py	12.25	1	−0.96	±0.05	−1.36	±0.04	−0.95	±0.02
		2	−0.93	±0.10	−1.43	±0.03		
SBB-MC#111-py	17.25	1	−1.09	±0.04	−1.49	±0.03	−0.97	±0.11
		1	−0.96	±0.03	−1.36	±0.03		
		2	−0.88	±0.04	−1.29	±0.03		
SBB-MC#113-py	22.25	1	−1.04	±0.08	−1.51	±0.08	−0.98	±0.09
		1	−0.92	±0.04	−1.25	±0.03		
SBB-MC#115-py	27.25	1	−1.22	±0.09	−1.72	±0.08	−1.02	±0.13
		1	−0.98	±0.05	−1.42	±0.03		
		2	−0.92	±0.04	−1.34	±0.04		
		2	−0.96	±0.05	−1.45	±0.04		
SBB-MC#117-py	32.25	1	−0.94	±0.04	−1.44	±0.03	−0.99	±0.07
		2	−1.04	±0.12	−1.44	±0.04		
Porewaters								
MC-MC#1-pw	0.50	1	−2.96	±0.04	−4.29	±0.04	−2.96	±0.04
MC-MC#4-pw	3.50	1	−1.41	±0.02	−1.96	±0.03	−1.40	±0.06
		1	−1.45	±0.07	−2.04	±0.07		
		2	−1.34	±0.10	−2.09	±0.05		
MC-MC#6-pw	5.50	1	−0.62	±0.03	−1.01	±0.03	−0.62	±0.03
MC-MC#8-pw	9.75	1	−1.33	±0.03	−1.91	±0.03	−1.33	±0.03
MC-MC#10-pw	14.75	1	−1.20	±0.03	−1.94	±0.03	−1.17	±0.03
		1	−1.16	±0.06	−1.63	±0.04		
		2	−1.14	±0.07	−1.64	±0.03		

(*continued on next page*)

Table 5 (*continued*)

Sample	Depth (cm)	Aliquot[a]	Individual analysis				Grand mean	
			δ^{56}Fe	2-SE	δ^{57}Fe	2-SE	δ^{56}Fe	1-SD[b]
MC-MC#12-pw	19.75	1	−1.90	±0.03	−2.78	±0.03	−1.95	±0.07
		2	−2.00	±0.10	−2.98	±0.07		
MC-MC#14-pw	24.75	1	−1.10	±0.04	−1.41	±0.03	−1.15	±0.06
		2	−1.19	±0.08	−1.73	±0.04		
MC-MC#16-pw	29.75	1	−1.29	±0.07	−1.87	±0.03	−1.25	±0.04
		2	−1.22	±0.03	−1.79	±0.03		
		2	−1.24	±0.04	−1.79	±0.03		
MC-MC#17-pw	32.25	1	−1.17	±0.02	−1.69	±0.02	−1.17	±0.02
MC-MC#20-pw	39.75	1	−2.69	±0.04	−3.88	±0.04	−2.69	±0.04
MC-MC#22-pw	44.75	1	−1.51	±0.03	−2.18	±0.04	−1.51	±0.03
MC-MC#24-pw	49.75	1	−1.49	±0.03	−2.06	±0.04	−1.49	±0.03
SBB-MC#101-pw	0.5	1	−1.82	±0.03	−2.71	±0.03	−1.82	±0.03
SBB-MC#103-pw	2.5	1	−0.94	±0.03	−1.35	±0.03	−0.94	±0.03
SBB-MC#105-pw	4.5	1	−0.81	±0.04	−1.22	±0.04	−0.81	±0.04
SBB-MC#107-pw	7.25	1	−0.35	±0.03	−0.50	±0.03	−0.35	±0.03
SBB-MC#109-pw	12.25	1	0.16	±0.02	0.26	±0.03	0.17	±0.00
		1	0.17	±0.03	0.36	±0.03		
SBB-MC#111-pw	17.25	1	−0.43	±0.04	−0.47	±0.03	−0.46	±0.04
		1	−0.49	±0.03	−0.67	±0.02		
SBB-MC#113-pw	22.25	1	0.41	±0.03	0.66	±0.03	0.31	±0.09
		1	0.26	±0.04	0.39	±0.03		
		1	0.25	±0.03	0.34	±0.03		
SBB-MC#115-pw	27.25	1	0.42	±0.10	0.71	±0.07	0.36	±0.07
		1	0.29	±0.04	0.53	±0.03		
		1	0.37	±0.03	0.62	±0.03		
SBB-MC#117-pw	32.25	1	0.33	±0.03	0.55	±0.03	0.33	±0.03

[a] Aliquot numbers refer to re-processed aliquot from original sample through separate chemical processing.
[b] For samples were only a single analysis was performed errors are cited as 2-SE for the individual analysis, which is typically the same as 1-SD.

oxidation occurs dominantly through anaerobic pathways. Bioturbation and bioirrigation promote re-oxidation of ferrous Fe-bearing phases, and this process tends to maintain sediments in a suboxic condition, which enhances DIR rates (Aller and Rude, 1988; Canfield et al., 1993; Thamdrup and Canfield, 1996; Thamdrup, 2000). Canfield et al. (1993) estimated that individual Fe atoms may undergo hundreds of oxidation–reduction cycles before ultimate burial. Mineralogical products of DIR include magnetite (Fe_3O_4) (Karlin et al., 1987; Lovley et al., 1987), and magnetite concentrations in the order of 0.1 dwt.% that have been measured in continental margin sediments might be a product of DIR (Canfield and Berner, 1987).

An alternative mineralogical product of DIR is siderite ($FeCO_3$), but in marine sediments its presence is considered anomalous because of its thermodynamic instability in the presence of sulfide and therefore its rarity in environments where bacterial sulfate reduction (BSR) occurs (Coleman et al., 1993). The sediment's dark brown to black color and strong sulfidic smell during the HCl extraction of sediments from both sites further suggests that most $Fe(II)_{HCl}$ is FeS and not siderite.

The relatively high magnetite abundances throughout the surface sediments at the MC locality, the evidence for bioturbation, high porewater $Fe(II)_{aq}$ and the low concentration of pyrite (Figs. 1–3) combined suggest that DIR plays an important role in organic carbon oxidation at this site. Thamdrup (2000) observed a consistent, positive correlation between relative rates of DIR and the concentration of poorly crystalline Fe(III) in sediments from different sites. This apparent co-variation suggests that as much as ~90% of total carbon oxidation may occur through DIR if concentrations of poorly crystalline Fe(III) exceed 30 μmol cm^{-3}. Assuming a sediment porosity of 0.8, sediments from the MC site contain an average of 30 μmol cm^{-3} of poorly crystalline Fe(III). Surface sediments from the SBB contain as much as 63 μmol cm^{-3} of poorly crystalline Fe(III), but this concentration decreases with depth and $Fe(III)_{HR}$ is absent below 10 cm (Fig. 2). These observations suggest that a significant proportion of organic carbon is respired through DIR in the upper 40 cm at the MC site, but that DIR is restricted to the surface few centimeters at the SBB site.

BSR is interpreted to be the primary pathway by which organic carbon oxidation occurs throughout most of the SBB core. Bioturbation is probably restricted to the upper few millimeters of the sediment surface at the SBB site, as indicated by the drop in ^{210}Pb contents (Fig. 3). Magnetite is almost absent throughout the core, and pyrite constitutes up to 56% of Fe_{HR}. Porewater $Fe(II)_{aq}$ becomes depleted to concentrations <40 μM below 9 cm (Fig. 1), coincident with the depth at which highly reactive Fe(III) becomes exhausted (Fig. 2), and this is interpreted to be the maximum depth at which DIR could be important in the

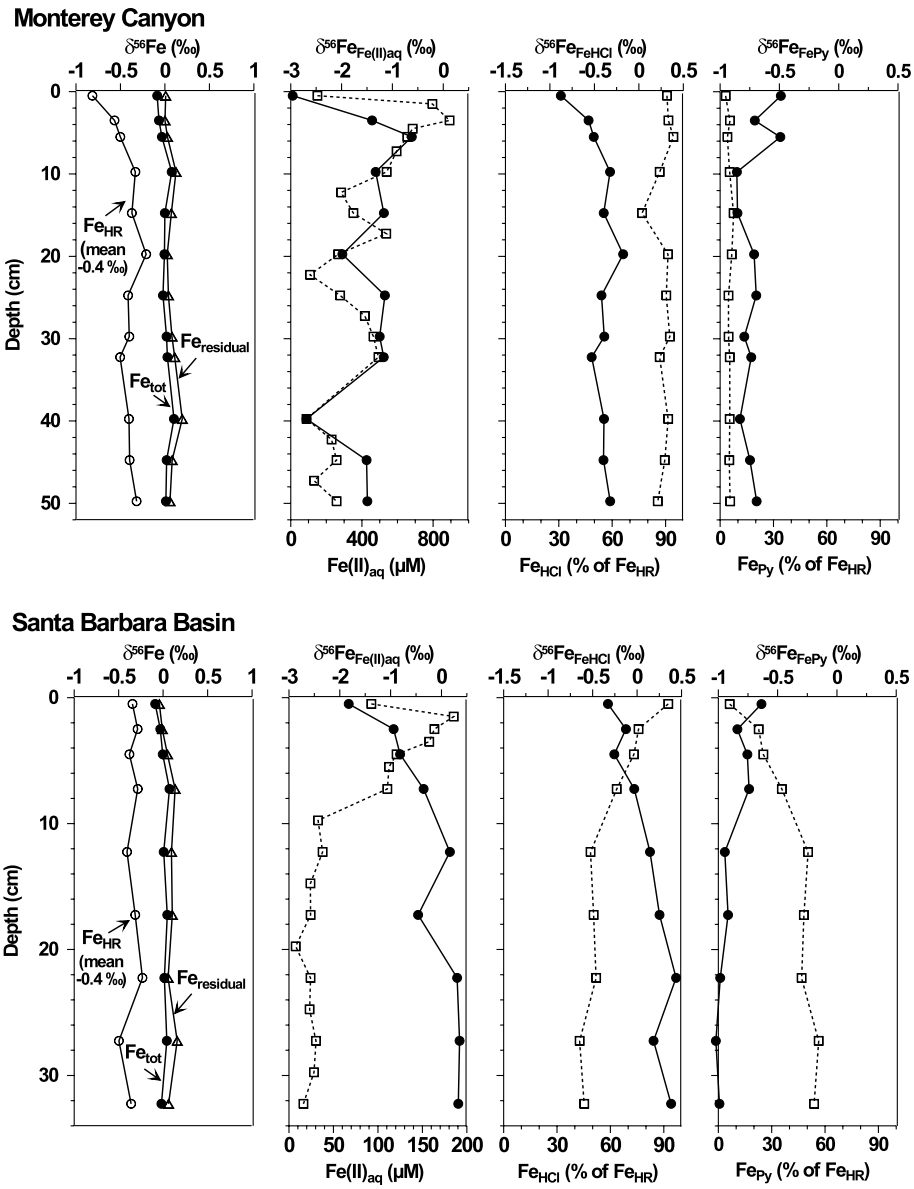

Fig. 4. Fe isotope compositions of Fe_{tot}, porewater $Fe(II)_{aq}$, HCl-extractable Fe, and pyrite (filled symbols). The HCl-extractable Fe fraction includes Fe(III) phases as well as FeS and possibly non-S Fe(II) solid phases, but not pyrite. The isotope composition of Fe_{HR} is calculated as the sum of the highly reactive Fe fractions ($Fe(II)_{aq}$, Fe_{HCl}, and Fe_{Py}), and the isotope composition of the residual Fe is calculated by mass balance. Open squares with dashed lines show the concentrations from Figs. 1 and 2. The difference in the dominant pathways of organic carbon oxidation between the two sites is reflected in the Fe isotope variations of the highly reactive Fe pool, and most notably in the Fe isotope compositions of $Fe(II)_{aq}$.

electron transport budget. These observations collectively suggest that BSR is important in the SBB core of this study, which is consistent with the results of Reimers et al. (1996), who measured high rates of BSR in SBB sediments using standard radiotracer techniques. The lack of bioturbation and the dominance of BSR likely facilitated pyrite formation, which, due to its low solubility and reactivity, is the ultimate end product of BSR in the presence of reactive Fe.

Paradoxically, sulfate concentrations in the surface 160 cm at the SBB site decrease only slightly from surface values, whereas in the MC sediments sulfate decreases markedly to a minimum of 3.4 mM over the 150 cm depth of the core (Fig. 1). This observation implies that absolute BSR rates at the MC site were high, significantly exceeding BSR activity in the SBB sediments. The contrasting sulfate porewater profiles from our two stations are consistent with the interpretation that overall rates of microbial carbon respiration are much higher in the MC sediments. It is surprising, however, that a large proportion of sulfide apparently escapes re-oxidation in this dynamic environment, and further, that the FeS in not converted to pyrite. Assuming that all $Fe(II)_{HCl}$ is FeS, which is likely to be an overestimate, the MC sediments have an average FeS–S/pyrite–S ratio of 5.6, distinctly higher than the ratios measured for most marine sediments, which are less than unity

(Howarth and Jørgensen, 1984; Morse and Cornwell, 1987; Thode-Andersen and Jørgensen, 1989; Fossing and Jørgensen, 1990; Middelburg, 1991; Reimers et al., 1996). High FeS–S/pyrite–S ratios have been reported from the suboxic/anoxic sediments of the Sagueney Fjord, Canada (FeS–S/pyrite–S ratios of 0.08 to 7.2; Gagnon et al., 1995) and the anoxic Orca basin (FeS–S/pyrite–S ratios of 1.6 to 26.9; Hurtgen et al., 1999). Conversion of FeS to pyrite may be inhibited by limited availability of S intermediates (Gagnon et al., 1995), and we speculate that a similar mechanism is operating here.

In summary, the high FeS–S/pyrite–S ratios inferred from the MC site, the co-existence of significant amounts of highly reactive Fe(III) and FeS to $\geqslant$50 cm depth and the irregular shapes of the $Fe(II)_{aq}$, sulfate and ammonia porewater profiles suggest that the sediments and pore fluids are not at steady-state. We infer that the MC sediments have been affected by non-diffusive transport processes such as bioirrigation or sediment slumping on the canyon walls. Despite some remaining uncertainties in the interpretation of the diagenetic boundary conditions, relevant points with respect to the interpretation of the Fe isotope data are: (a) between 10% and 51% of highly reactive Fe pool in the surface 50 cm of the MC sediments is ferric Fe, whereas in SBB sediments ferric Fe is deplete below ~10 cm depth, and (b) pyrite concentrations are low in MC sediments, whereas in SBB pyrite concentrations increase rapidly with depth. Further, we suggest that, despite the significant gradient in sulfate concentrations in the MC core, both BSR and DIR were active in the MC sediments. In the SBB sediments DIR is probably limited to the surface few centimeters, and BSR is the dominant carbon oxidation pathway below. However, net rates of BSR are higher at the MC site compared to SBB sediments.

5.2. Principal controls on Fe isotope compositions

The HCl-extractable fraction is the major component of the highly reactive Fe pool we have analyzed for Fe isotope compositions at the MC locality, and it remains the major component in the upper half of the sediment column at the SBB locality (Fig. 2). Although it is possible to measure the concentration of FeS operationally by analyzing the Fe(II) and the acid-volatile sulfide contents of the HCl-extractable sediment component, there is no extraction technique that can physically separate the Fe(III) and FeS fractions from the highly reactive Fe pool so that the Fe isotope composition of FeS may be exclusively determined. We can, however, explore the isotopic compositions of these two fractions in a mixing diagram (Fig. 5). The δ^{56}Fe values of the HCl extractions that have >80% Fe(II) are interpreted to lie close to those of FeS, and we estimate that FeS at both localities has δ^{56}Fe values between −0.4‰ and +0.4‰, where the higher δ^{56}Fe values appear to be associated with the SBB locality (Fig. 5). At both localities, however, the δ^{56}Fe values for FeS are significantly higher than those of pyrite, in the order of 1‰ based on the average

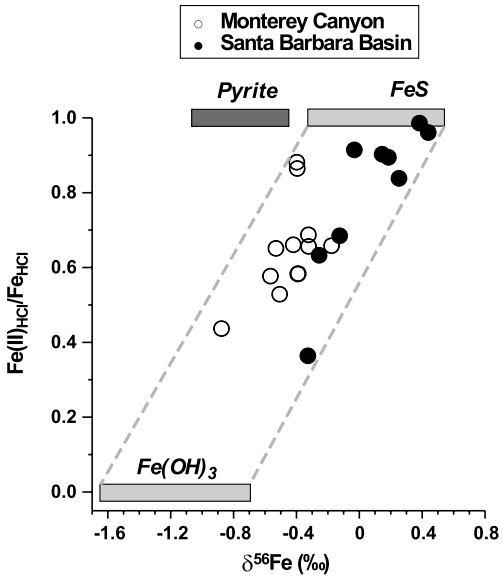

Fig. 5. Mixing diagram of $Fe(II)_{HCl}/Fe_{HCl}$ ratios versus $\delta^{56}Fe_{HCl}$, which provides a means for distinguishing end-member Fe isotope compositions of ferrous and ferric Fe in the highly reactive Fe pool. Based on samples that have $Fe(II)_{HCl}/Fe_{HCl}$ ratios $\geqslant$0.8, the data indicate that the δ^{56}Fe value of the solid Fe(II) component, which likely is dominated by FeS, varies between ~ −0.4‰ and ~ +0.4‰. The δ^{56}Fe values for the Fe(III) component in the HCl extractions are less well constrained because of the paucity of data at low $Fe(II)_{HCl}/Fe_{HCl}$ ratios, but the general trend suggests that the highly reactive ferric component has δ^{56}Fe values between −1.7‰ and −0.7‰.

compositions in Fig. 5, suggesting an Fe isotope fractionation during conversion of precursor FeS to pyrite.

Constraining the likely δ^{56}Fe values for the pure Fe(III) component in the HCl extractions is more difficult because few samples have >50% Fe(III), but the $Fe(II)_{HCl}/Fe_{HCl}$–δ^{56}Fe trends suggest that the Fe(III) component has very low δ^{56}Fe values, between −1.7‰ and −0.7‰ (Fig. 5). This conclusion is surprising given the expectation that the δ^{56}Fe values of ferric Fe-bearing species are generally higher than those of ferrous Fe-bearing species (Polyakov and Mineev, 2000; Schauble et al., 2001; Beard and Johnson, 2004; Johnson et al., 2004; Anbar et al., 2005). In addition, such low δ^{56}Fe values for ferric hydroxides contrast with the initial detrital values near zero. We take these observations to indicate that extensive Fe cycling has occurred in an open system.

The δ^{56}Fe values for $Fe(II)_{aq}$ decrease with increasing % Fe(III) in the highly reactive Fe pool (Fig. 6), which we interpret to reflect mixing between sulfide-dominated diagenesis and Fe cycling due to DIR at high % Fe(III). Pore fluids in the SBB samples where the highly reactive Fe is almost entirely Fe(II) have the highest δ^{56}Fe values, and this is taken as the end member for sulfide-dominated diagenesis. These samples have the lowest $Fe(II)_{aq}$ contents at the SBB site, between 16 and 38 μM (Fig. 6), consistent with control by low-solubility sulfide minerals. Using the estimated range in δ^{56}Fe values of −0.4‰ to +0.4‰ for FeS from Fig. 5 and the experimentally determined $Fe(II)_{aq}$–

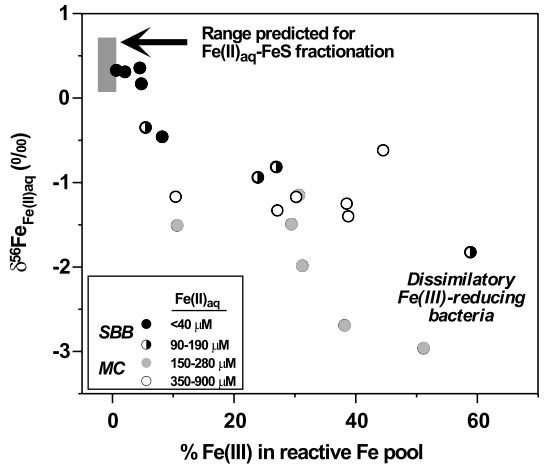

Fig. 6. Variations in δ^{56}Fe values for $Fe(II)_{aq}$ relative to the % Fe(III) in the highly reactive Fe pool as sampled by the HCl extraction δ^{56}Fe values for porewater Fe(II) decrease at both the MC and SBB sites with increasing % Fe(III) in the reactive Fe pool, suggesting variable contributions from sulfide-dominated diagenesis, which produces high-δ^{56}Fe values for $Fe(II)_{aq}$, and Fe oxide/hydroxide-dominated diagenesis, which produces low-δ^{56}Fe values for $Fe(II)_{aq}$. The later reflects DIR-catalyzed cycling. Note that the lowest δ^{56}Fe values in the MC sediments are associated with the lowest $Fe(II)_{aq}$ concentrations, reflecting the relative mass balance between the highly reactive $Fe(II)_{aq}$ and Fe(III) reservoirs.

FeS fractionation of +0.3‰ reported by Butler et al. (2005), $Fe(II)_{aq}$ in isotopic equilibrium with FeS would be expected to have δ^{56}Fe values between −0.1‰ and +0.7‰, which overlap those measured in the SBB samples that are interpreted to reflect the sulfide-dominated end member (Fig. 6).

The greatest amount of Fe cycling due to DIR is expected in the sections that have the greatest % Fe(III) in the highly reactive Fe pool (Fig. 2), and these samples have the lowest δ^{56}Fe values for $Fe(II)_{aq}$ (Fig. 6). Experimental studies of Fe isotope fractionation produced by DIR consistently indicate that the δ^{56}Fe values for $Fe(II)_{aq}$ are 1‰ to 2‰ lower than the initial ferric oxide/hydroxide before reduction (Beard et al., 1999; Beard et al., 2003b; Icopini et al., 2004; Crosby et al., 2005; Johnson et al., 2005). Although Icopini et al. (2004) proposed that sorption of Fe(II) might provide an abiologic mechanism for producing low-δ^{56}Fe $Fe(II)_{aq}$, they did not directly measure the Fe isotope compositions of sorbed Fe(II). Crosby et al. (2005) directly measured the $Fe(II)_{sorb}$–$Fe(II)_{aq}$ fractionation and determined that it is much less than that inferred by Icopini et al. (2004) and concluded that in general sorption of Fe(II) to ferric oxide/hydroxide surfaces cannot explain the low-δ^{56}Fe values for $Fe(II)_{aq}$ that are observed in DIR experiments. We therefore conclude that the low-δ^{56}Fe values for $Fe(II)_{aq}$ in the SBB and MC samples are produced during isotopic exchange between co-existing Fe(III) and $Fe(II)_{aq}$ pools and reflect Fe cycling that has been catalyzed by DIR.

Within the general trend of decreasing δ^{56}Fe for $Fe(II)_{aq}$ and increasing % Fe(III) in the highly reactive Fe pool is a tendency for the lowest δ^{56}Fe values to be associated with the lowest $Fe(II)_{aq}$ contents in the MC sediments (Fig. 6), which can also be seen in the profiles of Fig. 4. Crosby et al. (2005) noted that the Fe isotope fractionations produced during DIR reflect isotopic partitioning between reactive Fe(III) in the ferric oxide/hydroxide substrate and $Fe(II)_{aq}$, coupled to electron exchange, and that the absolute δ^{56}Fe values for $Fe(II)_{aq}$ reflect the relative mass balance of the $Fe(II)_{aq}$ and reactive Fe(III) reservoirs. When $Fe(II)_{aq}$ is a minor component, for example, the results of Crosby et al. (2005) predict that the δ^{56}Fe values should shift to strongly negative values, and this is observed in the data for the pore fluids.

The distinct Fe isotope compositions of FeS and pyrite (Fig. 5) may reflect an intrinsic isotope fractionation between these species and/or a pathway dependence in the isotopic fractionations involved in pyrite formation. In addition, the apparent $Fe(II)_{aq}$–pyrite fractionations measured at both the MC and SBB localities are significantly different than the theoretical fractionation that is obtained using the β factor for $Fe^{II}(H_2O)_6^{2+}$ from Schauble et al. (2001) and the β factor for pyrite from Polyakov and Mineev (2000), which predict a $Fe(II)_{aq}$–pyrite fractionation of -4.5 ± 1.5‰ at 20 °C. In contrast, we measure apparent $Fe(II)_{aq}$–pyrite fractionations between −2.5‰ and +1.5‰. Our results indicate that the Fe isotope composition of reactive Fe undergoes significant modification during early diagenesis and in particular during formation of sulfides. The origin of low-δ^{56}Fe values for pyrite at both sites is not yet clear, given the lack of experimental determination of Fe isotope fractionation factors for pyrite. The average δ^{56}Fe value for pyrite from our study is -0.78 ± 0.15‰, indicating that low-δ^{56}Fe pyrite may form in modern anoxic diagenetic environments. Although these values are not as low as those measured for Archean-age sedimentary pyrite by Rouxel et al. (2005), which has an average δ^{56}Fe value of -1.68 ± 0.90‰, our results show that low-δ^{56}Fe pyrite is not exclusive to Archean environments.

6. Conclusions

Large isotopic variations of up to 3.4‰ in $^{56}Fe/^{54}Fe$ ratios in suboxic to anoxic sediments from the California continental margin likely reflect a combination of biologically influenced processes. On balance the evidence suggests that the low δ^{56}Fe values of $Fe(II)_{aq}$ in the porewaters in sediments that contain ferric hydroxides are produced by DIR. Isotopic exchange between $Fe(II)_{aq}$ and highly reactive ferric phases, catalyzed by DIR, dominates the isotope composition of porewater $Fe(II)_{aq}$ in the MC sediments. Oxidation that accompanies extensive bioturbation and bioirrigation provides a recharge mechanism for ferric hydroxides that may be used as the terminal electron acceptor. Continental margin sediments that undergo intense suboxic Fe-recycling are expected to produce a significant benthic $Fe(II)_{aq}$ flux, and these results show that

such fluxes may have very low δ^{56}Fe values, significantly lower than those of mid-ocean ridge hydrothermal fluids (Sharma et al., 2001; Beard et al., 2003b; Severmann et al., 2003). Benthic $Fe(II)_{aq}$ fluxes therefore offer a possible explanation for the very low δ^{56}Fe values that appear to characterize Fe–Mn crusts near continental margins (Levasseur et al., 2004). Extensive biologically mediated Fe redox cycling appears to produce low δ^{56}Fe values for highly reactive Fe(III) oxide/hydroxide minerals, which contrasts with the near-zero δ^{56}Fe values that characterize the detrital flux of these minerals to the sediment column.

In contrast, the relatively anoxic sediments in the Santa Barbara basin (SBB) contain significant ferric hydroxides only in the upper few cm, and this is accompanied by low δ^{56}Fe values for porewater $Fe(II)_{aq}$ that occurs only in the upper portion of the sediment column. At depth the δ^{56}Fe values for porewater $Fe(II)_{aq}$ increase as diagenetic processes become increasingly sulfide dominated.

The observed Fe isotope compositions in the highly reactive Fe pool, which includes $Fe(II)_{aq}$, ferric hydroxides, FeS and pyrite, cannot be explained through simple mineral precipitation under equilibrium conditions. The large negative $Fe(II)_{aq}$–pyrite fractionations of $-5.0‰$ to $-3.8‰$ at low temperatures (5–50 °C) that are predicted by Polyakov and Mineev (2000) and Schauble et al. (2001) do not follow the observed isotopic differences between these components at the MC and SBB localities, suggesting possible pathway dependence in sulfide formation, fluid–mineral disequilibrium, errors in the predicted fractionations, or a combination of these. Although observed $Fe(II)_{aq}$–FeS fractionations are generally far from the $+0.3‰$ fractionation that is interpreted by Butler et al. (2005) to approach equilibrium conditions, they converge toward the experimentally determined value when the reactive Fe pool is dominated by sulfide and is almost entirely ferrous Fe.

Our results demonstrate that large Fe isotope variations that span the entire range yet measured on Earth may be produced in modern marine sediments through DIR and Fe sulfide formation. In the case of DIR, low-δ^{56}Fe $Fe(II)_{aq}$ and reactive Fe(III) solid phases reflect extensive redox cycling of Fe. For sulfide-dominated Fe cycling, which is ultimately driven by BSR, relatively high δ^{56}Fe values are produced for FeS and especially $Fe(II)_{aq}$, reflecting isotopic exchange between these species. The distinct Fe isotope compositions involved in the DIR and sulfide-dominated pathways provide a framework for interpreting Fe isotope variations in ancient marine sedimentary rocks (Johnson et al., 2003; Matthews et al., 2004; Rouxel et al., 2005; Yamaguchi et al., 2005).

Acknowledgments

We greatly appreciate the efforts of the captain and crew of the R/V *Point Sur*, in particular we thank Steward Lamerdin for his enthusiastic support. Chris Moser, Dale Hubbard, Chris Holm, and Andy Ross all helped with the sampling and analysis during the cruise and ashore. Special thanks go to Geoff Wheat and Sam Hulme for providing additional equipment and man-power during the cruise. Support for S. Severmann, C.M. Johnson, and B.L. Beard was provided by funding from the NASA-Ames Research Center and the NASA Astrobiology Institute through a Joint Research Initiative (JRI NCC 2-5449) and the National Science Foundation (EAR-0106614). Funding for sample collection was provided to J. McManus from the National Science Foundation (OCE-0219651). Constructive criticism by three anonymous reviewers and the Associate Editor, Tim Lyons, have helped to refine our discussion and are greatly appreciated.

Associate editor: Timothy W. Lyons

References

Albarède, F., Beard, B.L., 2004. Analytical methods for non-traditional isotopes. In: Johnson, C.M., Beard, B.L., Albarède, F. (Eds.), *Geochemistry of Non-Traditional Stable Isotopes*, vol. 55. Mineralogical Society of America and Geochemical Society, pp. 113–152.

Aller, R.C., Mackin, J.E., Cox Jr., R.T., 1986. Diagenesis of Fe and S in Amazon inner shelf muds: apparent dominance of Fe reduction and implications for the genesis of ironstones. *Cont. Shelf Res.* **6**, 263–289.

Aller, R.C., Rude, P.D., 1988. Complete oxidation of solid phase sulfides by manganese and bacteria in anoxic marine sediments. *Geochim. Cosmochim. Acta* **52**, 751–765.

Anbar, A.D., Jazecki, A.A., Spiro, T.G., 2005. Theoretical investigation of iron isotope fractionation between $Fe(H_2O)_6^{3+}$ and $Fe(H_2O)_6^{2+}$: implications for stable isotope geochemistry. *Geochim. Cosmochim. Acta* **69**, 825–837.

Beard, B., Johnson, C.M., Cox, L., Sun, H., Nealson, K.H., Aguilar, C., 1999. Iron isotope biosignatures. *Science* **285**, 1889–1896.

Beard, B.L., Johnson, C.M., 2004. Fe isotope variations in the modern and ancient Earth and other planetary bodies. In: Johnson, C.M., Beard, B.L., Albarède, F. (Eds.), *Geochemistry of Non-Traditional Stable Isotopes*, vol. 55. Mineralogical Society of America and Geochemical Society, pp. 319–357.

Beard, B.L., Johnson, C.M., Skulan, J.L., Nealson, K.H., Sun, H., Cox, L., 2003a. Application of Fe isotopes to tracing the geochemical and biochemical cycling of Fe. *Chem. Geol.* **195**, 87–117.

Beard, B.L., Johnson, C.M., Von Damm, K.L., Poulson, R.L., 2003b. Iron isotope constraints on Fe cycling and mass balance in the oxygenated Earth oceans. *Geology* **31**, 629–632.

Behl, R.J., Kennett, J.P., 1999. Brief interstadial events in the Santa Barbara basin, NE Pacific, during the past 60 kyr. *Nature* **379**, 243–246.

Berelson, W.M., McManus, J., Coale, K.H., Johnson, K.S., Burdige, D.J., Kilgore, T., Colodner, D., Chavez, F.P., Kudela, R., Boucher, J., 2003. A time series of benthic flux measurements from Monterey Bay, CA. *Cont. Shelf Res.* **23**, 457–481.

Berner, R.A., 1970. Sedimentary pyrite formation. *Am. J. Sci.* **268**, 1–23.

Brantley, S.L., Liermann, L., Bullen, T.D., 2001. Fractionation of Fe isotopes by soil microbes and organic acids. *Geology* **29**, 535–538.

Brantley, S.L., Liermann, L., Guynn, R.L., Anbar, A.D., Icopini, G.A., Barling, J., 2004. Fe isotopic fractionation during mineral dissolution with and without bacteria. *Geochim. Cosmochim. Acta* **68**, 3189–3204.

Bruland, K.W., Franks, R.P., Landing, W.M., Soutar, A., 1981. Southern California inner basin sediment trap calibration. *Earth Planet. Sci. Lett.* **53**, 400–408.

Bullen, T.D., White, A.F., Childs, C.W., Vivit, D.V., Schulz, M.S., 2001. Demonstration of significant abiotic iron isotope fractionation in nature. *Geology* **29**, 699–702.

Butler, I.B., Archer, C., Vance, D., Olroyd, A., Rickard, D.T., 2005. Fe isotope fractionation on FeS formation in ambient aqueous solution. *Earth Planet. Sci. Lett.* **236**, 430–442.

Canfield, D.E., 1989. Reactive iron in marine-sediments. *Geochim. Cosmochim. Acta* **53**, 619–632.

Canfield, D.E., Berner, R.A., 1987. Dissolution and pyritization of magnetite in anoxic marine sediments. *Geochim. Cosmochim. Acta* **51**, 645–659.

Canfield, D.E., Des Marais, D.J., 1993. Biogeochemical cycles of carbon, sulfur, and free oxygen in a microbial mat. *Geochim. Cosmochim. Acta* **57**, 3971–3984.

Canfield, D.E., Thamdrup, B., Hansen, J.W., 1993. The anaerobic degradation of organic matter in Danish coastal sediments: Iron reduction, manganese reduction, and sulfate reduction. *Geochim. Cosmochim. Acta* **57**, 3867–3883.

Cline, J.D., 1969. Spectrophotometric determination of hydrogen sulfide in natural waters. *Limnol. Oceanogr.* **14**, 454–458.

Coleman, M.L., Hedrick, D.B., Lovley, D.R., White, D.C., Pye, K., 1993. Reduction of Fe(III) in sediments by sulphate-reducing bacteria. *Nature* **361**, 436–438.

Croal, L.R., Johnson, C.M., Beard, B.L., Newman, D.K., 2004. Iron isotope fractionation by Fe(II)-oxidizing photoautotrophic bacteria. *Geochim. Cosmochim. Acta* **68**, 1227–1242.

Crosby, H.A., Johnson, C.M., Roden, E.E., Beard, B.L., 2005. Fe(II)–Fe(III) electron/atom exchange as a mechanism for Fe isotope fractionation during dissimilatory iron oxide reduction. *Environ. Sci. Technol.* **39**, 6698–6704.

Dierssen, H., Balzer, W., Landing, W.M., 2001. Simplified synthesis of an 8-hydroxyquinoline chelating resin and a study of trace metal profiles from Jellyfish Lake, Palau. *Mar. Chem.* **73**, 173–192.

Elrod, V.A., Berelson, W.M., Coale, K.H., Johnson, K.S., 2004. The flux of iron from continental shelf sediments: A missing source for global budgets. *Geophys. Res. Lett.* **31**, L12307. doi:10.1029/2004GL020216.

Fantle, M.S., DePaolo, D.J., 2004. Iron isotopic fractionation during continental weathering. *Earth Planet. Sci. Lett.* **228**, 547–562.

Fossing, H., Jørgensen, B.B., 1990. Oxidation and reduction of radiolabelled inorganic sulfur compounds in an estuarine sediment, Kysing Fjord, Denmark. *Geochim. Cosmochim. Acta* **54**, 2731–2742.

Froelich, P.N., Klinkhammer, G.P., Bender, M.L., Luedtke, N.A., Health, G.R., Cullen, D., Dauphin, P., Hammond, D.E., Hartman, B., Maynard, V., 1979. Early organic matter in pelagic sediments of the eastern equatorial Atlantic: suboxic diagenesis. *Geochim. Cosmochim. Acta* **43**, 1075–1090.

Gagnon, C., Mucci, A., Pelletier, E., 1995. Anomalous accumulation of acid-volatile sulphides (AVS) in a coastal marine sediment, Saguenay Fjord, Canada. *Geochim. Cosmochim. Acta* **59**, 2663–2675.

Gilmore, G., Hemingway, J.D., 1995. *Practical Gamma-Ray Spectrometry*. John Wiley and Sons, 314 pp.

Howarth, R.W., Jørgensen, B.B., 1984. Formation of ^{35}S-labelled elemental sulfur and pyrite in coastal marine sediments (Limfjorden and Kysing Fjord, Denmark) during short-term $^{35}SO_4^{2-}$ reduction measurements. *Geochim. Cosmochim. Acta* **48**, 1807–1818.

Huerta-Diaz, M.A., Morse, J.W., 1990. A quantitative method for determination of trace metal concentrations in sedimentary pyrite. *Mar. Chem.* **29**, 119–144.

Hurtgen, M.T., Lyons, T.W., Ingall, E.D., Cruse, A.M., 1999. Anomalous enrichments of iron monosulfide in euxinic marine sediments and the role of H_2S in iron sulfide transformations; examples from Effingham Inlet, Orca Basin, and the Black Sea. *Am. J. Sci.* **299**, 556–588.

Icopini, G.A., Anbar, A.D., Ruebush, S.S., Tien, M., Brantley, S.L., 2004. Iron isotope fractionation during microbial reduction of iron: The importance of adsorption. *Geology* **32**, 205–208.

Johnson, C.M., Beard, B.L., Beukes, N.J., Klein, C., O'Leary, J.M., 2003. Ancient geochemical cycling in the Earth as inferred from Fe isotope studies of Banded Iron Formations from the Transvaal Craton. *Contrib. Mineral. Petrol.* **144**, 523–547.

Johnson, C.M., Beard, B.L., Roden, E.E., Newman, D.K., Nealson, K.H., 2004. Isotopic contraints on biogeochemical cycling of Fe. In: Johnson, C.M., Beard, B.L., Albarède, F. (Eds.), *Geochemistry of Non-Traditional Stable Isotopes*, vol. 55. Mineralogical Society of America and Geochemical Society, pp. 359–408.

Johnson, C.M., Roden, E.E., Welch, S.A., Beard, B.L., 2005. Experimental constraints on Fe isotope fractionation during magnetite and Fe carbonate formation coupled to dissimilatory hydrous ferric oxide reduction. *Geochim. Cosmochim. Acta* **69**, 963–993.

Johnson, C.M., Skulan, J.L., Beard, B.L., Sun, H., Nealson, K.H., Bratermann, P.S., 2002. Isotopic fractionation between Fe(III) and Fe(II) in aqueous solutions. *Earth Planet. Sci. Lett.* **195**, 141–153.

Karlin, R.E., Lyle, M., Heath, G.R., 1987. Authigenic magnetite formation in suboxic marine sediments. *Nature* **326**, 490–493.

Kennett, J.P., Ingram, B.L., 1995. A 20,000-year record of ocean circulation and climate change from the Santa Barbara basin. *Nature* **377**, 510–514.

Koide, M., Soutar, A., Goldberg, E.D., 1972. Marine geochronology with ^{210}Pb. *Earth Planet. Sci. Lett.* **14**, 442–446.

Kostka, J.E., Luther, G.W., 1994. Partitioning and speciation of solid iron in saltmarsh sediments. *Geochim. Cosmochim. Acta* **58**, 1701–1710.

Laës, A., Blain, S., Laan, P., Achterberg, E.P., Sarthou, G., de Baar, H.J.W., 2003. Deep dissolved iron profiles in the eastern North Atlantic in relation to water masses. *Geophys. Res. Lett.* **30**, 1902. doi:10.1029/2003GL017902.

Lapp, B., Balzer, W., 1993. Early diagenesis of trace metals used as an indicator of past productivity changes in coastal sediments. *Geochim. Cosmochim. Acta* **57**, 4639–4652.

Levasseur, S., Frank, M., Hein, J.R., Halliday, A.N., 2004. The global variations in the iron isotope composition of marine hydrogenetic ferromanganese deposits: Implications for seawater chemistry? *Earth Planet. Sci. Lett.* **224**, 91–105.

Lovley, D.R., Stolz, J.F., Nord, G.L.J., Phillips, E.J.P., 1987. Anaerobic production of magnetite by a dissimilatory iron-reducing microorganism. *Nature*, 252–254.

Martin, J.H., 1990. Glacial-interglacial CO_2 changes: The iron hypothesis. *Paleoceanography* **5**, 1–13.

Matthews, A., Morhans-Bell, H.S., Emmanuel, S., Jenkyns, H., Erel, Y., Halciz, L., 2004. Controls of iron-isotope fractionation in organic-rich sediments (Kimmeridge Clay, Upper Jurassic, southern England). *Geochim. Cosmochim. Acta* **68**, 3107–3123.

McManus, J., Berelson, W.M., Coale, K.H., Johnson, K.S., Kilgore, T., 1997. Phosphorous regeneration in continental margin sediments. *Geochim. Cosmochim. Acta* **61**, 2891–2907.

Middelburg, J.J., 1991. Organic carbon, sulphur, and iron in recent semi-euxinic sediments of Kau Bay, Indonesia. *Geochim. Cosmochim. Acta* **55**, 815–828.

Morford, J.L., Emerson, S.R., 1999. The geochemistry of redox sensitive trace metals in sediments. *Geochim. Cosmochim. Acta* **63**, 1735–1750.

Morse, J.W., 1994. Interactions of trace metals with authigenic sulfide minerals—implications for their bioavailability. *Mar. Chem.* **46**, 1–6.

Morse, J.W., Cornwell, J.C., 1987. Analysis and distribution of iron sulfide minerals in recent anoxic marine sediments. *Mar. Chem.* **22**, 55–69.

Parsons, T.R., Maita, Y., Lalli, C.M., 1984. *A Manual of Chemical Seawater Analysis*. Pergamon Press, 173 pp.

Pilskaln, C.H., Paduan, J.B., Chavez, F.P., Anderson, R.Y., Berelson, W.M., 1996. Carbon export and regeneration in the coastal upwelling system of Monterey Bay, central California. *J. Mar. Res.* **54**, 1149–1178.

Polyakov, V.B., Mineev, S.D., 2000. The use of Mössbauer spectroscopy in stable isotope geochemistry. *Geochim. Cosmochim. Acta* **64**, 849–865.

Poulton, S.W., 2003. Sulfide oxidation and iron dissolution kinetics during the reaction of dissolved sulfide with ferrihydrite. *Chem. Geol.* **202**, 79–94.

Poulton, S.W., Krom, M.D., Raiswell, R., 2004. A revised scheme for the reactivity of iron (oxyhydr)oxide minerals towards dissolved sulfide. *Geochim. Cosmochim. Acta* **68**, 3703–3715.

Pyzik, A.J., Sommer, S.E., 1981. Sedimentary iron monosulfides—kinetics and mechanism of formation. *Geochim. Cosmochim. Acta* **45**, 687–698.

Raiswell, R., Buckley, F., Berner, R.A., Anderson, T.F., 1988. Degree of pyritisation of iron as a paleoenvironmental indicator of bottom-water oxygenation. *J. Sed. Petrol.* **58**, 812–819.

Raiswell, R., Canfield, D.E., Berner, R.A., 1994. A comparison of iron extraction methods for the determination of degree of pyritisation and the recognition of iron-limited pyrite formation. *Chem. Geol.* **111**, 101–110.

Reimers, C.E., Ruttenberg, K.C., Canfield, D.E., Christiansen, M.B., Martin, J.B., 1996. Porewater pH and authigenic phases formed in the uppermost sediments of the Santa Barbara Basin. *Geochim. Cosmochim. Acta* **60**, 4037–4057.

Rouxel, O., Bekker, A., Edwards, K.J., 2005. Iron isotope constraints on the Archean and Paleoproterozoic ocean redox state. *Science* **307**, 1088–1091.

Rouxel, O., Dobbek, N., Ludden, J., Fouquet, Y., 2003. Iron isotope fractionation during oceanic crust alteration. *Chem. Geol.* **202**, 155–182.

Rouxel, O., Fouquet, Y., Ludden, J., 2004. Subsurface processes at the Lucky Strike hydrothermal field, Mid-Atlantic Ridge: Evidence from sulfur, selenium, and iron isotopes. *Geochim. Cosmochim. Acta* **68**, 2295–2311.

Ruttenberg, K.C., Berner, R.A., 1993. Authigenic apatite formation and burial in sediments from nonupwelling, continetal margin environments. *Geochim. Cosmochim. Acta* **57**, 991–1007.

Schauble, E.A., Rossman, G.R., Taylor, H.P., 2001. Theoretical estimates of equilibrium Fe-isotope fractionations from vibrational spectroscopy. *Geochim. Cosmochim. Acta* **65**, 2487–2497.

Severmann, S., German, C.R., Edmonds, H.N., Beard, B.L., Johnson, C.M., 2003. The modification of hydrothermal Fe-isotopic signature during plume-processes. *Geochim. Cosmochim. Acta* **67**, A424.

Severmann, S., Johnson, C.M., Beard, B.L., German, C.R., Edmonds, H.N., Chiba, H., Green, D.R.H., 2004. The effect of plume processes on the Fe-isotope composition of hydrothermally derived Fe in the deep ocean as inferred from the Rainbow vent site, Mid-Atlantic Ridge, 36° 14′N. *Earth Planet. Sci. Lett.* **225**, 63–76.

Sharma, M., Polizzotto, M., Anbar, A.D., 2001. Iron isotopes in hot springs along the Juan de Fuca Ridge. *Earth Planet. Sci. Lett.* **194**, 39–51.

Shaw, T.J., Gieskes, J., Jahnke, R.A., 1990. Early diagenesis in differing depositional environments: The response of transition metals in pore water. *Geochim. Cosmochim. Acta* **54**, 1233–1246.

Sholkovitz, E., 1973. Intersitial water chemistry of the Santa Barbara sediments. *Geochim. Cosmochim. Acta* **37**, 2043–2073.

Skulan, J.L., Beard, B.L., Johnson, C.M., 2002. Kinetic and equilibrium isotope fractionation between aqueous Fe(III) and hematite. *Geochim. Cosmochim. Acta* **66**, 2995–3015.

Sørensen, J., Jørgensen, B.B., 1987. Early diagenesis in sediments from Danish coastal waters: Microbial activity and Mn–Fe–S geochemistry. *Geochim. Cosmochim. Acta* **51**, 1583–1590.

Stookey, L.L., 1970. Ferrozine—a new spectrophotometric reagent for iron. *Anal. Chem.* **42**, 779–781.

Thamdrup, B., 2000. Bacterial manganese and iron reduction in aquatic sediments. In: Schink, B. (Ed.), *Advances in Microbial Ecology*, vol. 16. Kluwer Academic/Plenum Publisher, pp. 41–84.

Thamdrup, B., Canfield, D.E., 1996. Pathways of carbon oxidation in continental margin sediments off central Chile. *Limnol. Oceanogr.* **41**, 1629–1650.

Thamdrup, B., Fossing, H., Jørgensen, B.B., 1994. Manganese, iron, and sulfur cycling in a coastal marine sediment, Aarhus Bay, Denmark. *Geochim. Cosmochim. Acta* **58**, 5115–5129.

Thode-Andersen, S., Jørgensen, B.B., 1989. Sulfate reduction and the formation of ^{35}S-labelled FeS, FeS_2, and S^0 in coastal marine sediments. *Limnol. Oceanogr.* **34**, 793–806.

Thomson, J., Higgs, N.C., Colley, S., 1996. Diagenetic redistribution of redox-sensitive elements in northeast Atlantic glacial/interglacial transition sediments. *Earth Planet. Sci. Lett.* **139**, 365–377.

Thunell, R.C., Tappa, E., Anderson, D.M., 1995. Sediment fluxes and varve formation in Santa Barbara Basin. *Geology* **23**, 1083–1086.

Welch, S.A., Beard, B.L., Johnson, C.M., Bratermann, P.S., 2003. Kinetic and equilibrium Fe isotope fractionation between aqueous Fe(II) and Fe(III). *Geochim. Cosmochim. Acta* **67**, 4231–4250.

Wiesli, R.A., Beard, B.L., Johnson, C.M., 2004. Experimental determination of Fe isotope fractionation between aqueous Fe(II), Siderite, and ''Green Rust'' in abiotic systems. *Chem. Geol.* **211**, 343–362.

Yamaguchi, K.E., Johnson, C.M., Beard, B.L., Ohmoto, H., 2005. Biogeochemical cycling of iron in the Archean-Paleoproterozoic Earth: Constraints from iron isotope variations in sedimentary rocks from the Kaapvaal and Pilbara Cratons. *Chem. Geol.* **218**, 135–169.

Zheng, Y., Anderson, R.F., Van Geen, A., Kuwabara, J., 2000. Authigenic molybdenum formation in marine sediments: A link to pore water sulfide in the Santa Barbara Basin. *Geochim. Cosmochim. Acta* **64**, 4165–4178.

Zhu, X.K., O'Nions, R.K., Guo, Y., Reynolds, B.C., 2000. Secular variations of iron isotopes in North Atlantic Deep Water. *Science* **287**, 2000–2002.